Full Title: Hypoxia-inducible-factors differentially contribute to clinical disease and the control of viral replication during RSV infection

Running Title: Investigating HIF-1α and HIF-2α during RSV infection

Authors: Dorothea R. Morris[a,b,c], Yue Qu[c], Yava L. Jones-Hall[d], Teodora Ivanciuc[c], Tianshuang Liu[c], Roberto P. Garofalo[a,c], Antonella Casola[a,c#]

[a]Department of Microbiology & Immunology, The University of Texas Medical Branch, Galveston, TX, USA

[b]School of Population & Public Health, The University of Texas Medical Branch, Galveston, TX, USA

[c]Department of Pediatrics, The University of Texas Medical Branch, Galveston, TX, USA

[d]School of Veterinary Medicine and Biomedical Science, Texas A&M University, College Station, TX, USA

#Address correspondence to AC, ancasola@utmb.edu; DRM, dormorri@utmb.edu

Abstract word count: 248/250

Importance word count: 147/150

Abstract: Hypoxia-inducible-factors (HIF) are transcription factors that regulate cellular adaptation to hypoxic conditions, enabling cells to survive in low-oxygen environments. Viruses have evolved to stabilize this pathway to promote successful viral infection, therefore modulation of HIFs could represent a novel antiviral strategy. In previous *in vitro* studies, we demonstrate respiratory syncytial virus (RSV), a leading cause of respiratory illness, to stabilize HIFs under normoxic conditions, with inhibition of HIF-1α resulting in reduced viral replication. Despite several HIF modulating compounds being tested/approved for use in other non-infectious models, little is known about their efficacy against respiratory viruses using relevant animal models. This study aimed to characterize the disease modulating properties and antiviral potential of anti-HIF-1α (PX478) and anti-HIF-2α (PT2385) in RSV-infected BALB/c mice. We found inhibition of HIF-1α to worsen clinical disease parameters, while simultaneously improving airway function. Additionally, anti-HIF-1α results in significantly reduced viral titer at early and peak time points of RSV replication, followed by a loss in viral clearance when given every day, but not every-other-day. In contrast, inhibition of HIF-2α was associated with improved clinical parameters, with no changes in airway function, and amelioration of interstitial pneumonia. Furthermore, anti-HIF-2α reduced early and peak lung viral replication, with no impaired viral clearance. Analysis of lung cells found significant modification in the T cell compartment that correlated with changes in lung pathology and viral titers in response to each HIF inhibitor administration. These data underscore the complex role of HIFs in RSV infection and highlight the need for careful therapeutic consideration.

Importance: The pharmacological use of HIF therapeutics has largely been investigated with various models of cancer, autoimmunity, and non-infectious lung damage. The safety and success of these compounds is emphasized by their use in several phase-4 clinical trials. Since the early 2000s, numerous studies have demonstrated the antiviral potential of HIF inhibitors in epithelial cell lines, however, there are no studies characterizing the therapeutic outcomes of suppressing HIF during a viral respiratory infection in a relevant animal model. With the growing interest in drug repositioning, our research emphasizes the importance of testing approved or abandoned therapeutics under the new conditions in a complex biological model encompassing both the epithelial and immune compartments. Moreover, the current study uncovers a novel role of HIFs in the pathogenesis of RSV disease. These data collectively demonstrate a key mechanism in immune regulation during RSV infection that can further therapeutic development.

Introduction: Respiratory syncytial virus (RSV) is a prominent cause of respiratory infections among infants, young children, and the elderly. Each year, there are an estimated 33 million infections and 150,000 deaths [1]. There is no available therapeutic agent for RSV infection and only recently two effective vaccines have been approved for use in elderly patients [2]. These same vaccines have been shown to limit severe disease in children but are not as efficient at preventing RSV infection as they are in the elderly [3,4]. Further research into effective therapeutics and broadening our understanding of the pathology of RSV is important to protecting these vulnerable populations.

As an obligate intracellular pathogen, viruses must rely on host cell machinery to establish productive infections. Many viruses have been shown to modify cellular metabolism to achieve virion assembly by increasing sources of energy and generating pools of free nucleotides, amino

acids, lipid materials, and glycoproteins [5]. Our laboratory recently demonstrated RSV to divert core metabolic activity towards the glycolytic pathway in a hypoxia-inducible-factor (HIF)-1α dependent manner [6]. HIFs are transcription factors that regulate the expression of a wide range of target genes in response to low oxygen levels [7]. These target genes have crucial roles in diverse biological processes, enabling cells to adapt and survive under hypoxic conditions. The HIF complex is a heterodimer consisting of an inducible α subunit (HIF-1α, HIF-2α, or HIF-3α) and a constitutively expressed β subunit (HIF-1β) [8]. While there is overlap in their functionality, the HIF-α isoforms also exhibit distinct transcriptional regulation in response to hypoxia and disease states [9-11]. HIF-1α is the most extensively studied isoform of the HIF family. Expressed in nearly all cell types, HIF-1α is the master regulator of cellular and systemic responses to hypoxia. Genes activated by HIF-1α modify a broad range of processes including energy metabolism, angiogenesis, epithelial-mesenchymal transition (EMT), and immune cell regulation [9,11]. HIF-2α exhibits a more limited distribution, predominately expressed in specific organs such as the kidney, liver, and lung. Genes upregulated by HIF-2α are primarily involved in erythropoiesis, vascular development, and iron metabolism[11]. HIF-3α is the most recent of the HIF isoforms to be described. Because of this, the precise distribution and function of HIF-3α is still being investigated.

As the gatekeeper to a diverse biological network, the use of the HIF pathway allows many viruses to create a cellular environment that favors viral replication, persistence, and immune evasion. The manipulation of this pathway has been observed with several DNA- and RNA viruses, even under oxygen-rich conditions [12,13]. The significance of HIF in cancer pathology has led much of the existing literature to focus on viruses known to induce tumor formation as part of their pathogenic mechanism [12,13]. Surprisingly, limited research has explored the clinical

manifestations and antiviral potential of HIF therapeutics against respiratory viral infections [12-15].

In addition to shifts in glycolytic metabolism, we previously observed RSV to stabilize both HIF-1α and HIF-2α in primary small airway epithelial cells [6]. We found the therapeutic inhibition of HIF-1α, but not HIF-2α, to result in promising antiviral activity. Given the implications for HIF in both the epithelial and immune compartments, we now seek to understand the involvement of HIFs in RSV pathology by utilizing inhibitors of HIF-1α and HIF-2α in a BALB/c mouse model. Here in, we reveal the novel involvement of HIFs in the development of RSV disease, shedding new light on its pathogenesis. Moreover, we demonstrate a key mechanism in immune regulation during RSV infection that can further therapeutic development.

Results:

Inhibition of HIF-1α during RSV infection results in worsening clinical disease and schedule-dependent regulation of RSV replication. To investigate whether inhibition of HIF-1α affects clinical disease, groups of BALB/c mice were administered PX478 at a dose of 20mg/kg by oral gavage. Mice received PX478 either every 24 h (PXQD) or every 48 h (PXQAD) over the 10-day infection period (Fig. 1A). Shortly after the first dose of PX478, mice were anesthetized and intranasally (IN) infected with RSV at a dose of $5x10^6$ plaque forming units (PFU). We found mice that received PXQD, regardless of infection status, to have worsening body weight and illness score, characterized by an inability to regain weight (Fig. 1B). When the treatment regimen was adjusted to PXQAD, the uninfected mice that received PX478 no longer exhibited substantial weight-loss or illness in comparison to the PBS/PBS mice (Fig. 1C). Despite this, RSV infected mice treated with PXQAD continued to demonstrate significantly worse body weight-loss and

illness score in comparison to the RSV/PBS mice, but showed signs of recovery at the later stages of the disease course.

We next evaluated viral replication following HIF-1α inhibition at days 2, 4, 7, and 10 post-infection (p.i.) by plaque assay. RSV infected mice treated with PXQD were found to have significantly reduced RSV replication at early and peak time points of days 2 (1.40 Log reduction) and 4 p.i. (0.81 Log reduction), respectively (Fig. 1D). Interestingly, at day 7 p.i., a timepoint of known RSV clearance, replication in PXQD mice was maintained at a similar level to day 4. By day 10 p.i., RSV replication remained detectable in some RSV/PXQD mice with an average of 1.40 log. RSV infected mice that received PXQAD had similar reductions in RSV replication at days 2 (1.37 log reduction) and 4 p.i. (2.27 log reduction). At days 7 and 10 p.i., no virus was detected in RSV/PXQAD mice, consistent with successful clearance of RSV from the lung tissue (Fig. 1E). These data collectively demonstrate HIF-1α to be important for protection from RSV induced disease and suggests HIF-1α has a complex role in regulating RSV replication.

HIF-1α is critical for the induction of the immune response following RSV infection. To understand the impact of HIF-1α inhibition on the immune response, we first evaluated the cellular composition of the BAL fluid. Uninfected mice that received PXQD or PXQAD showed no significant alterations to BAL cellular composition as compared to the respective PBS/PBS control groups (Fig. 2A-2H). RSV infected mice that received PXQD demonstrated significant reductions in the number of total cells present in the BAL (Fig. 2A), specifically, in the number of lymphocytes (Fig. 2B) and macrophages (Fig. 2C) at all time points tested. Neutrophil cell counts showed a trend for reduced cell numbers but were not significantly altered as compared to the RSV/PBS control mice (Fig. 2D). RSV infected mice that received PXQAD showed similar patterns in cellular composition, with total cell counts (Fig. 2E), lymphocytes (Fig. 2F), and

macrophages (Fig. 2G) being significantly reduced, though to a slightly lesser extent when compared to RSV/PXQD mice. Neutrophil cell counts were significantly reduced at day 2 p.i. but remained similar to the RSV/PBS control mice at all other time points (Fig. 2H). Together, these data suggest HIF-1α is critical for the presence of immune cells within the airway space.

We next investigated whether the pattern of decreased immune activity observed in the BAL had an impact on the T-cell population in the lung tissue, given the crucial role for $CD4^+$ and $CD8^+$ T-cells in controlling RSV replication and clearance [16-18]. Flow cytometry analysis was performed on whole lung tissue collected at days 4 and 7 p.i. as depicted in Fig. S1. Starting with $CD4^+$ T-cells, we observed significant reductions at day 4 p.i. in $CD4^+$ naïve cells (Fig. 3A), $CD4^+$ effector cells (Fig. 3B), active $CD4^+$ T-cells (Fig. 3C), and $CD4^+$ Treg cells (Fig. 3D) in RSV/PXQD mice as compared to the RSV/PBS control mice with fold reductions of 1.5, 3.3, 3.4, and 2.1 respectively. For RSV/PXQAD mice, similar reductions in $CD4^+$ effector cells (Fig. 3B) and active $CD4^+$ T-cells (Fig. 3C) were also appreciated with fold reductions of 2.8 and 2.1, respectively. Comparative analysis between RSV/PXQD and RSV/PXQAD mice at day 4 p.i. found a significantly greater reduction of $CD4^+$ naive cells, $CD4^+$ effector T-cells, and $CD4^+$ Treg cells in RSV/PXQD mice (Fig. 3A, 3B, 3D). At day 7 p.i., $CD4^+$ effector cells and $CD4^+$ Treg cells remained significantly reduced in RSV/PXQD mice with a 2.8 and 2.4-fold reduction, respectively (Fig. 3A, 3D). All other $CD4^+$ cell counts in RSV/PXQD and RSV/PXQAD mice at day 7 p.i. were similar to the RSV/PBS control mice.

For $CD8^+$ T-cells, we observed significant reductions at day 4 p.i. in $CD8^+$ naïve cells for both RSV/PXQD and RSV/PXQAD mice with fold reductions of 1.9 and 1.3, respectively (Fig. 3E). Comparative analysis between RSV/PXQD and RSV/PXQAD at day 4 p.i. found a significantly greater reduction of $CD8^+$ naive cells in RSV/PXQD mice (Fig. 3E). At day 7 p.i.,

$CD8^+$ effector cells (Fig. 3F) and active $CD8^+$ T-cells (Fig. 3G) were significantly reduced in both RSV/PXQD and RSV/PXQAD mice as compared to RSV/PBS control mice. RSV/PXQD demonstrated fold reductions of 4.3 and 3.5, while RSV/PXQAD had fold reductions of 1.68 and 1.5, respectively. Comparative analysis between RSV/PXQD and RSV/PXQAD at day 7 p.i. found a significantly greater reduction of $CD8^+$ effector cells and active $CD8^+$ T-cell in RSV/PXQD mice (Fig. 3F, 3G). These data collectively demonstrate HIF-1α to have an integral role in T-cell function and activation during RSV infection.

Inhibition of HIF-1α improves airway function during RSV infection. To assess airway function during RSV infection, we first measured bronchoconstriction using whole-body plethysmography as previously described [19]. Uninfected mice that received PXQD or PXQAD showed no significant alterations to Penh values at any timepoint tested as compared to the respective PBS/PBS control groups (Fig. 4A, 4D). RSV infected mice that received PXQD or PXQAD had significant improvements in Penh at days 1, 5, and 6 p.i., with values similar to the PBS/PBS control mice throughout the disease course. We next measured total protein and LDH activity in the BAL fluid as an indicator of epithelial damage and generalized cell death, respectively. Uninfected mice that received PXQD or PXQAD showed no significant alterations to total protein or LDH activity at any timepoint tested as compared to the respective PBS/PBS control groups (Fig. 4B-4F). Interestingly, RSV infected mice that received PXQD demonstrated significant improvements at day 4 p.i. to total protein (Fig. 4B) and LDH activity (Fig. 4C). By day 10 p.i., these same mice were found to have an increasing trend in LDH activity as compared to the RSV/PBS control mice (Fig. 4C). RSV/PXQAD mice had similar improvements in total protein at day 4 p.i., but demonstrated moderate worsening of total protein levels at day 10 p.i. (Fig. 4E).

LDH activity in these mice remained comparable to the RSV/PBS control mice at all time points (Fig. 4F).

Lastly, we assessed the lung tissue of mice that received PXQAD by histopathology. Based on the scoring determined by a board-certified veterinarian with expertise in mouse lung morphology, uninfected mice that received PXQAD remained comparable to the PBS/PBS control mice at all time points tested (data not shown). RSV infected mice that received PXQAD had significant increases in the total lung score (Fig. 5A) that consisted of significant increases in the percent of abnormal lung field (Fig. 5B) and increased interstitial pneumonia (Fig. 5C) at the beginning of infection. At days 4 and 7 p.i., RSV/PXQAD mice demonstrated significant improvements in perivasculitis (Fig. 5D) and peribronchiolitis (Fig. 5E) as compared to the RSV/PBS control mice. By day 10 p.i., no significant differences to the lung tissue were noted. Representative images of the lung tissue for RSV/PBS and RSV/PXQAD mice are shown in Fig.6. Collectively, these data suggest HIF-1α to contribute to the worsening of airway function and tissue damage during the acute phase of RSV infection.

Inhibition of HIF-2α results in improved clinical disease and antiviral activity during RSV infection. While there exists a degree of functional overlap between the HIF-α subunits, they have also been demonstrated to distinctly govern a range of biological activities. Therefore, we wanted to better understand the role of HIF-2α during RSV infection. To do so, mice were administered PT2385 in DMSO+Corn-oil (CO) by oral gavage every 24 h at a dose of 50mg/kg (Fig. 7A). Shortly after the first dose of PT2385, mice were anesthetized and intranasally (IN) infected with RSV at a dose of $5x10^6$ PFU. Uninfected mice that received PT2385 were found to have similar body weight loss and illness score as the PBS/CO control mice (Fig. 7B). RSV infected mice that received PT2385 demonstrated significant improvements to bodyweight loss at nearly all

timepoints over the 10-day disease course as compared to the RSV/CO control mice (Fig. 7B). Interestingly, the illness score in RSV/PT2385 mice was initially worse, followed by a quicker recovery as compared to the RSV/CO control mice.

We next assessed viral replication following HIF-2α inhibition at days 2, 4, 7, and 10 p.i.. RSV infected mice treated with PT2385 showed significantly reduced RSV replication at early and peak timepoints with a 2.2 log reduction at day 2 p.i. and a 2.7 log reduction at day 4 p.i. (Fig. 7C). By days 7 and 10 p.i., no replicating virus was detected in RSV/PT2385 mice, indicating successful clearance of RSV from the lung tissue. Additionally, increasing doses of PT2385 up to 100 mg/kg did not alter viral clearance at days 7 and 10 p.i. (data not shown). These data collectively suggest HIF-2α to contribute to RSV induced disease and the promotion of viral replication.

Inhibition of HIF-2α leads to increased immune activity in the BAL and lung tissue of RSV infected mice. To understand the impact of HIF-2α inhibition on the immune response, we first evaluated the cellular composition of the BAL fluid. Uninfected mice that received PT2385 showed no significant alterations to BAL cellular composition as compared to the PBS/CO control groups (Fig. 8A-8D). RSV infected mice that received PT2385 demonstrated a significant increase in the number of total of cells present in the BAL (Fig. 8A), specifically, in the number of lymphocytes (Fig. 8B). Macrophage cell counts (Fig. 8C) were significantly increased at days 2 and 10 p.i., while neutrophil cell counts (Fig. 8D) were not significantly altered as compared to the RSV/CO control mice.

Given the antiviral activity in RSV/PT2385 mice, we assessed the T-cell population using flow cytometry analysis at days 4 and 7 p.i. as depicted in Fig. S1. Starting with $CD4^+$ T-cells, we observed an increasing trend at day 4 p.i. in $CD4^+$ naïve cells (Fig. 9A) as well as significant

increases in $CD4^+$ effector cells (Fig. 9B) and active $CD4^+$ T-cells (Fig. 9C) in RSV/PT2385 mice as compared to the RSV/CO control mice with fold increases of 1.2, 1.4 and 1.5, respectively. By day 7 p.i., all $CD4^+$ T-cells in the RSV/PT2385 were of comparable number to the RSV/CO control mice. Additionally, no changes in CD4+ Treg cells were appreciated at days 4 or 7 p.i. in RSV/PT2385 mice as compared to the RSV/CO control mice (Fig. 9D). For $CD8^+$ T-cells, we observed significant increases at day 4 p.i. in $CD8^+$ naïve cells (Fig. 9E), $CD8^+$ effector cells (Fig. 9F), and active $CD8^+$ cells (Fig. 9G) with fold increases of 1.4, 1.6, and 1.3, respectively. On day 7 p.i., the number of active $CD8^+$ T-cells remained significantly increased, while $CD8^+$ naïve and effector cell numbers were comparable to the RSV/CO control mice. Collectively, these data suggest HIF-2α functions to suppress T-cell responses during RSV infection.

HIF-2α inhibition does not modify airway function during RSV infection. To assess airway function during RSV infection, we first measured bronchoconstriction. Uninfected mice that received PT2385 showed no significant alterations to Penh values at any timepoint tested as compared to the PBS/CO control mice (Fig. 10A). Similarly, RSV infected mice treated with PT2385 had similar Penh values as the RSV/CO control mice throughout the 10-day disease course. We next measured total protein and LDH activity in the BAL. We observed no significant differences in total protein for all mice tested as compared to their respective control groups (Fig. 10B). Interestingly, RSV/PT2385 mice had significantly elevated LDH activity at days 2 and 4 p.i. (Fig. 10C), consistent with the moderate increase in immune cell numbers (Fig.8, Fig. 9). By day 7 p.i., LDH activity was comparable to the RSV/CO control mice. No significant differences in LDH activity were appreciated between PBS/PT2385 and the PBS/CO control mice at any timepoint tested.

Lastly, we assessed the lung tissue of mice that received PT2385 by histopathology. Based on the scoring determined by a board-certified veterinarian with expertise in mouse lung morphology, uninfected mice that received PT2385 remained comparable to the PBS/CO control mice at all time points tested (data not shown). For RSV infected mice treated with PT2385, the total lung score (Fig. 11A) was improved beginning at day 2 p.i., consisting of significant improvements to the percent of abnormal lung field (Fig. 11B). At days 4 and 7 p.i., no significant differences in any scored parameter were appreciated. By day 10 p.i., the lung tissue of RSV/PT2385 mice demonstrated significant worsening of perivasculitis (Fig. 11C), while having significant improvements in peribronchiolitis (Fig. 11D) and interstitial pneumonia (Fig. 11E). Representative images of the lung tissue for RSV/CO and RSV/PT2385 mice are shown in Fig.12. Together, these data suggest HIF-2α does not modify airway function but does contribute to worsening lung pathology during the acute phase of RSV infection.

Discussion: HIFs have been extensively studied in various models of cancer and non-infectious lung injury [14,20,21]. Investigations into the effects of HIFs during viral respiratory infection have been primarily limited to *in vitro* characterizations [15]. To date, no studies have been conducted investigating the therapeutic potential of a HIF inhibitor against a viral respiratory infection in an animal model. Our lab has previously demonstrated RSV to stabilize both HIF-1α and HIF-2α under normoxic conditions in primary small airway epithelial cells [6]. We also show inhibition of HIF-1α, but not HIF-2α, to have antiviral potential in these cells. Given the diverse biological role of HIFs, we next wanted to understand the function of these inhibitors in an animal model of RSV infection. In this study, we find the inhibition of HIF-1α by PX478 during RSV infection to worsen clinical disease. Anti-HIF-1α also resulted in antiviral activity in the lung tissue of RSV infected mice, though this was complicated by a schedule-dependent loss in viral clearance. We show this shift in viral clearance to likely be driven by a schedule-dependent reduction in $CD4^+$ and $CD8^+$ T-cells. In contrast, inhibition of HIF-2α by PT2385 was found to improve clinical disease with no major alteration to airway function. Anti-HIF-2α similarly resulted in antiviral activity following RSV infection with no impact to viral clearance. This antiviral activity is likely due to a heightened immune response, characterized by an increase in $CD4^+$ and $CD8^+$ T-cell activity. Taken together, these data emphasize a unique and complex role for HIFs in the context of RSV infection. Moreover, they offer new insight to how HIF inhibitors may be used as antiviral therapeutics in an *in vivo* model of viral respiratory infection.

During our initial piloting of PX478, we observed notable weight loss and increased illness in the PBS/PXQD mice compared to the PBS control mice. However, when analyzing various factors such as BAL cells, airway function, total protein, and LDH activity, we found no significant differences compared to the PBS control mice. This suggests that the deteriorating clinical

condition in PBS/PXQD mice is likely influenced by a factor other than inflammation or tissue damage. It's worth noting that, apart from the time interval, we are administering a dose similar to or less than what is reported in the literature [22-24]. Studies investigating the anti-tumor efficacy of PX478 have administered this compound for up to 5 consecutive days, reporting minor weight-loss in the mice during this time [24,25]. Based on our review, we believe we are the first to administer PX478 for longer than 5 consecutive days. Other cancer models have delivered PX478 every ~2-3 days for extended periods and report no negative effects in mice [26,27]. Moreover, PX478 has been well-tolerated by patients in a phase-1 clinical trial with the most common side effect reported to be nausea [28,29]. Interestingly, studies using obese mouse models have noted PX478 to prevent weight gain [30,31]. Additionally, a recent investigation has shown the efficacy of PX478 as a potential therapeutic for type-II diabetes [32]. Considering the significant role of HIF-1α in metabolic function and the recent repositioning of PX478 for treatment of type-II diabetes, it is probable that consecutive dosing of PX478 for extended periods of time may lead to appetite suppression. In our model, spacing treatments over 48 h ameliorated this effect, resulting in patterns of clinical disease in the PBS/PXQAD mice that resemble previously reported observations. Despite this, RSV infected mice treated with PX478 every 48 h continued to display delayed recovery as compared to the RSV control mice (Fig. 1C). This was surprising as these mice effectively cleared the virus from the lung tissue and show no signs of increased inflammatory activity. One possible explanation for the phenomenon could be a moderate appetite suppression that is amplified due to the stress of infection. Throughout the study, we continued to compare the two treatment regimens due to the unexpected effect on viral clearance.

In RSV-infected mice, inhibition of HIF-1α or HIF-2α showed antiviral activity. However, based on our previous characterizations in epithelial cells and the cellular responses noted in this

study, the mechanisms underlying this activity appear to be distinct for each HIF-α subunit [6]. Treatment with PX478 during RSV infection resulted in a suppressed immune response, suggesting that the antiviral activity is more likely attributed to impaired RSV entry or replication rather than immune-mediated clearance. A primary role of HIF-1α is to regulate metabolic activity within the cell [33]. Our lab and others have previously shown RSV infection to alter host cell metabolism, favoring glycolysis, and for this to be important for RSV replication [6,34,35]. Inhibition of HIF-1α in RSV infected mice may reduce the glycolytic capacity within lung epithelial cells, effecting replication. Additionally, RSV infection has been shown to induce autophagy and for the inhibition of this process to have profound impacts to RSV replication [36-38]. HIF-1α is instrumental in the autophagic pathway, inducing the expression of pro-autophagic genes like BNIP3 and BNIP3L/NIX, directly upregulating autophagy-related genes (ATG) such as ATG5, ATG7, and ATG12, and promoting proteins crucial for autophagosome formation [39,40]. In addition to shifts in metabolism, it is likely that the autophagy pathway is also disrupted due to HIF-1α inhibition, further contributing to reduced RSV replication.

In contrast to PX478, treatment with PT2385 results in a moderate increase in immune cell presence in RSV infected mice, characterized by heightened $CD4^+$ and $CD8^+$ T-cell number and activity. T-cells play a critical role in controlling RSV replication and clearance within the host [16-18]. $CD4^+$ effector cells are known to aid in the recruitment and activation of other immune cells that control RSV replication such as natural killer (NK) cells, $CD8^+$ cytotoxic T-cells, and B-cells [41-43]. $CD8^+$ effector cells are critical for the clearance of RSV infection from the lung tissue [44]. Therefore, it is probable that this increase in T-cell activity could explain the observed antiviral effects seen in RSV/PT2385 mice. Although, HIF-2α is known to have important roles in regulating immune responses, its specific contribution to T-cell function is not as extensively

studied as HIF-1α [45]. Recently, a loss of HIF-2α in regulatory T-cells (Treg) was described to reduce Treg suppressor functions leading to an increase in $CD4^+$ T-cell activity [46,47]. Additionally, a loss of HIF-2α did not alter Treg development [46,47]. Our results indicate an increase in $CD4^+$ and $CD8^+$ T-cell activity with no significant alteration to Treg cell numbers as compared to the RSV/PBS control mice, suggesting a potential loss in Treg suppressor activity. Furthermore, treatment of Tregs and $CD4^+$ T-cells with PT2385 was found to result in an increase in HIF-1α expression [47]. HIF-1α is a potent inducer of T-cell activation and migration. Collectively, this could explain the increase in generalized T-cell number and activity in our model as well as how PT2385 treatment led to an early control and clearance of RSV from the lung tissue. Moreover, it shows patients on this FDA-approved medication may have protection from viral respiratory infection.

On the other hand, mice treated with PX478 were observed to have a schedule-dependent loss in viral clearance in the lung tissue. As previously mentioned, PX478 treatment was observed to have a schedule-dependent reduction in T-cell number and activity. RSV infected mice that received PXQD were found to have significantly less $CD4^+$ and $CD8^+$ T-cells than RSV infected mice that received PXQAD. It is likely that RSV/PXQAD mice retained a T-cell threshold sufficient to clear the virus from the lung tissue. These findings have important implications as it suggests patients on anti-HIF-1α medication may experience enhanced disease during the course of viral respiratory infections.

HIF-1α has been demonstrated to impact airway function in a variety of ways, including the induction of bronchoconstriction [48]. HIF-1α achieves this by influencing the contractility of airway smooth muscles through several mechanisms such as stimulating calcium production, modulating ion channels, and triggering the release of mediators like leukotrienes [49-51]. In

contrast, HIF-2α has been shown to be dispensable for the induction of changes to airway hypersensitivity and bronchoconstriction [46]. Consistent with these findings, we observed notable improvements in bronchoconstriction in RSV-infected mice treated with PX478 but not with PT2385. Furthermore, HIFs have a crucial role in promoting tissue repair under hypoxic conditions but can also promote further injury depending on gene activation [52]. We find RSV/PXQAD mice to have an initial worsening of the lung field and increases in the severity of interstitial pneumonia (Fig. 5, 6). This could possibly be due to uncontrolled ROS production driven by the RSV infection at this timepoint [53]. HIF-1α is known to promote antioxidant activity, therefore inhibiting HIF-1α likely reduced the antioxidant capacity allowing for ROS induced by RSV replication to further damage the lung tissue [54]. During the intermediate timepoints where RSV replication has been reduced and cleared from the tissue, pathology scores for perivasculitis and peribronchiolitis are significantly improved as compared to the RSV control mice. By day 10 p.i., the lung tissue of RSV/PXQAD was comparable to the RSV/PBS control mice. HIF-1α has important roles at the later stages of lung injury in promoting angiogenesis and tissue regeneration [52]. Therefore, it is likely that inhibition of HIF-1α at the later stages of disease may hinder proper tissue repair, negating the benefit gained prior. Mice treated with PT2385 during RSV infection had an initial improvement in the appearance of the lung field. Until day 10 p.i., no major alterations to any scored category were appreciated. By the end of the acute phase, RSV/PT2385 mice had moderate increases in perivasculitis, but significant improvements in all other categories. This increase in perivasculitis is consistent with increases in the number of immune cells within the BAL and lung tissue. Improvements in the other categories could be due to the resolution of RSV infection by this timepoint.

In conclusion, our data demonstrate a novel and complex role for HIF-1α and HIF-2α in the context of RSV infection. Though many have shown the antiviral potential of HIF-1α *in vitro*, the current study underscores the importance of continued investigation using complex models that encompass both the epithelial and immune compartments. Additionally, we highlight anti-HIF-2α as a potential therapeutic option for RSV. Moreover, we have established a valuable reference point for comparing HIF-related responses in other viral respiratory infections. Future investigations will focus on further understanding the underlying mechanistic contribution of HIFs to the immune response and tissue repair process during RSV infection.

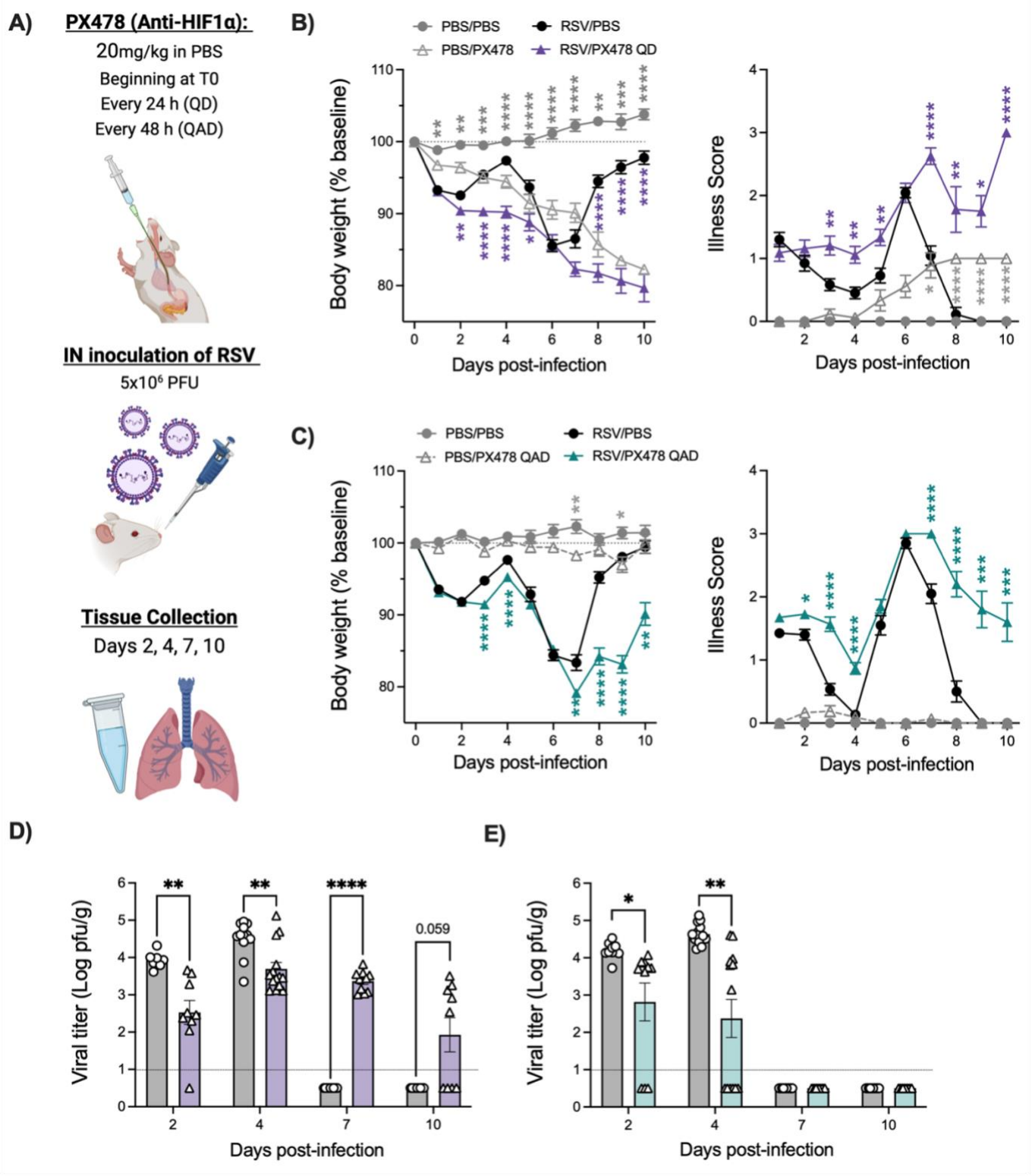
A)
PX478 (Anti-HIF1α):
20mg/kg in PBS
Beginning at T0
Every 24 h (QD)
Every 48 h (QAD)
IN inoculation of RSV
5x10⁶ PFU
Tissue Collection
Days 2, 4, 7, 10
B)
PBS/PBS
RSV/PBS
PBS/PX478
RSV/PX478 QD
Body weight (% baseline)
Days post-infection
Illness Score
C)
PBS/PBS
RSV/PBS
PBS/PX478 QAD
RSV/PX478 QAD
Body weight (% baseline)
Days post-infection
Illness Score
D)
Viral titer (Log pfu/g)
0.059
Days post-infection
E)
Viral titer (Log pfu/g)
Days post-infection

Fig 1. *Assessment of clinical disease and viral replication following HIF-1α inhibition during RSV infection.* (A) The experimental design for Figures 1-6. Detailed descriptions can be found in the methods section. Mice received PX478 either (B, D) every 24 h or (C, E) every 48 h over the 10-day infection period. (B, C) All mice were monitored daily for changes in bodyweight loss and illness score. (D-E) At days 2, 4, 7, and 10 p.i., the right lung was collected for assessment of viral replication by plaque assay. For clinical disease, data are pooled from four independent experiments ($n \leq 75$ mice/group). For viral replication, data are pooled from two independent experiments ($n \leq 14$ mice/group). Data are expressed as mean ± SEM. Significant results were determined by two-way ANOVA or mixed effects analysis (* $p \leq 0.05$, ** $p \leq 0.01$, *** $p \leq 0.001$, **** $p \leq 0.0001$).

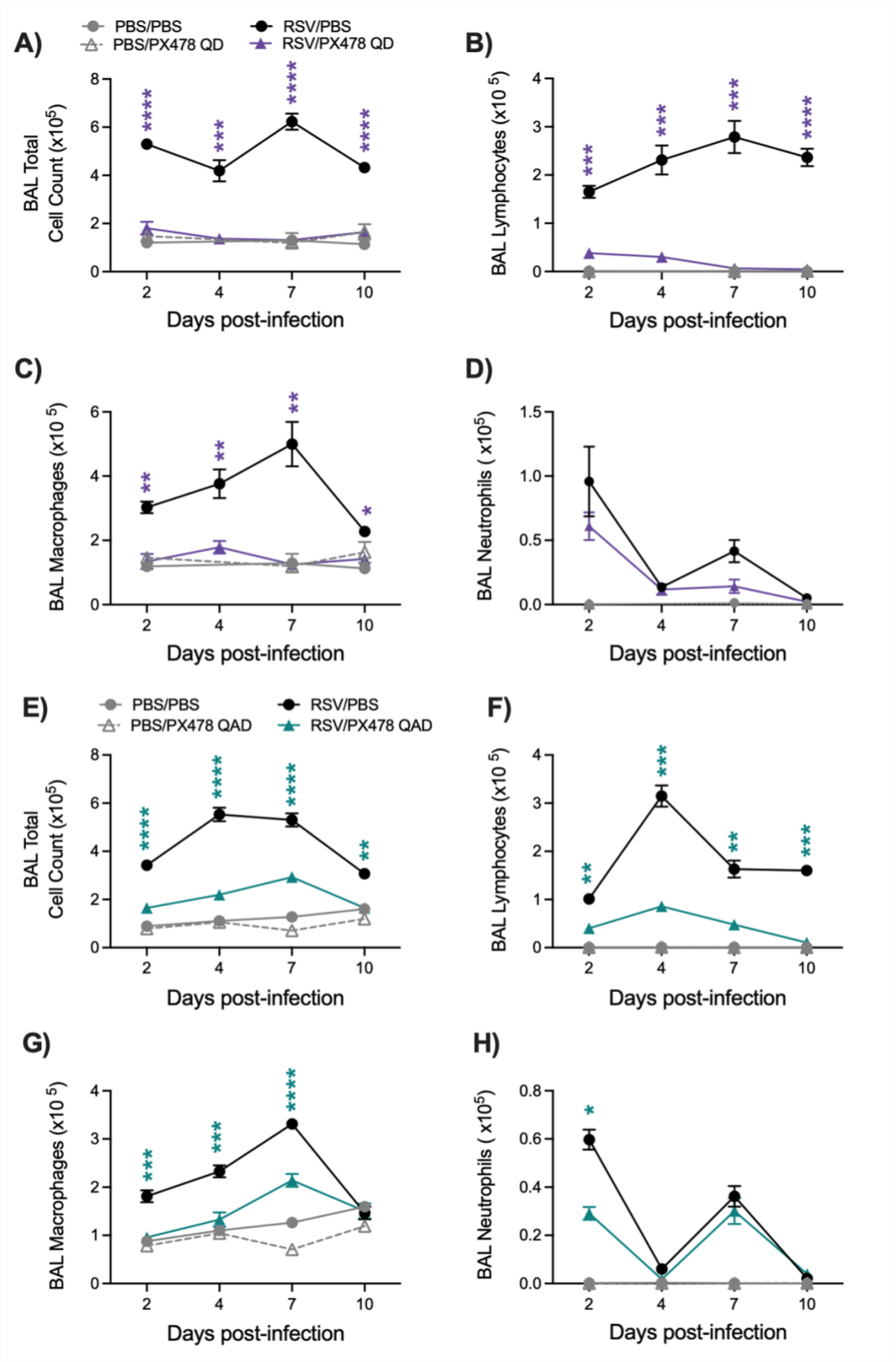
A)
PBS/PBS
PBS/PX478 QD
RSV/PBS
RSV/PX478 QD
BAL Total Cell Count (x10^5)
Days post-infection
B)
BAL Lymphocytes (x10^5)
Days post-infection
C)
BAL Macrophages (x10^5)
Days post-infection
D)
BAL Neutrophils (x10^5)
Days post-infection
E)
PBS/PBS
PBS/PX478 QAD
RSV/PBS
RSV/PX478 QAD
BAL Total Cell Count (x10^5)
Days post-infection
F)
BAL Lymphocytes (x10^5)
Days post-infection
G)
BAL Macrophages (x10^5)
Days post-infection
H)
BAL Neutrophils (x10^5)
Days post-infection

386

Fig 2. *Differential cell count of the BAL fluid following HIF-1α inhibition during RSV infection.* At days 2, 4, 7, or 10 p.i., BAL fluid was collected from mice that had received PX478 either (A-D) every 24 h or (E-H) every 48 h over the 10-day infection period. This was used to obtain (A, E) total cell counts, as well as differential cell counts consisting of (B, F) lymphocytes, (C, G) macrophages, and (D, H) neutrophils. Data are pooled from two independent experiments ($n \leq 15$ mice/group). Data are expressed as mean ± SEM. Significant results were determined by mixed-effects analysis (* $p \leq 0.05$, ** $p \leq 0.01$, *** $p \leq 0.001$, **** $p \leq 0.0001$).

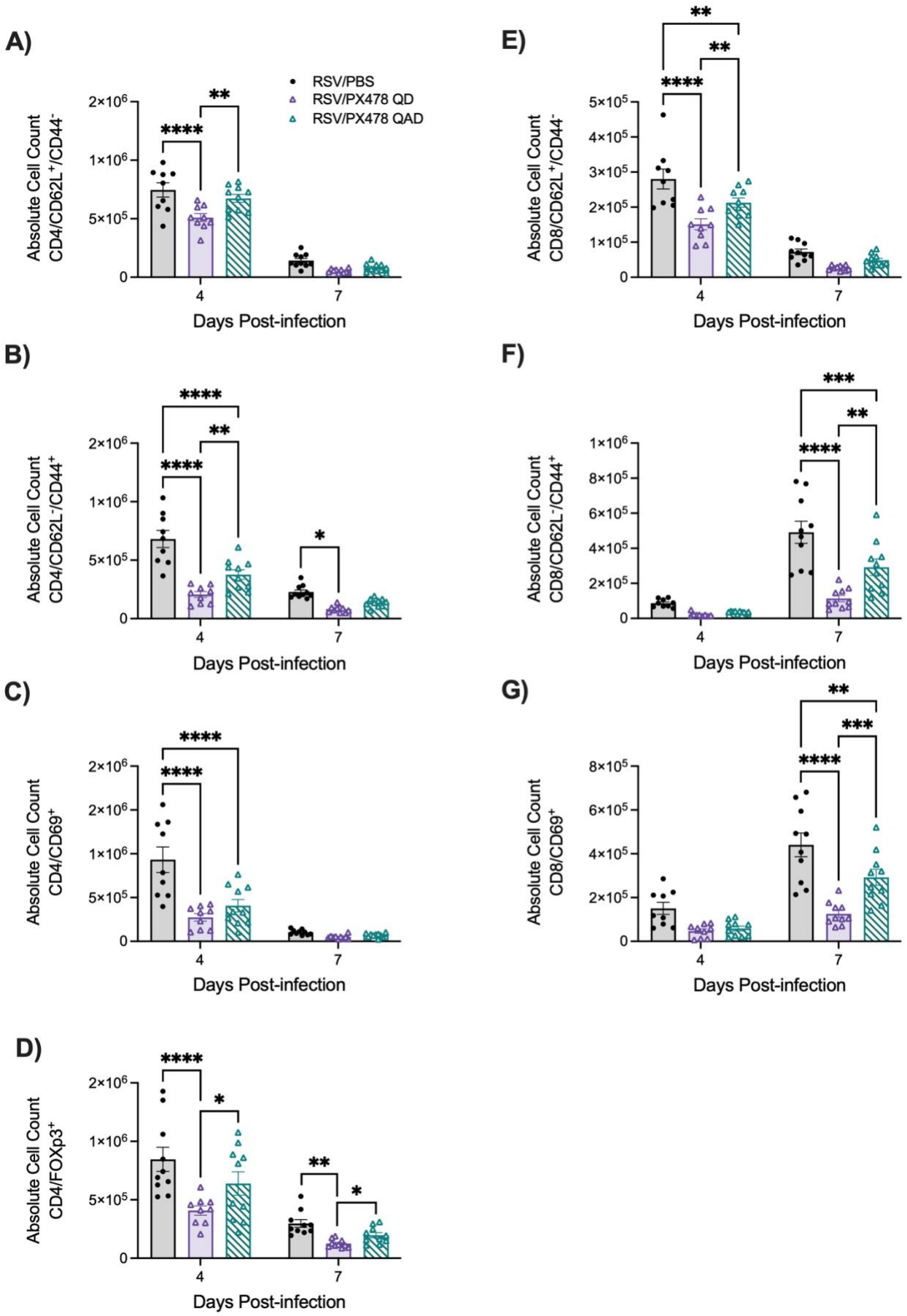
A)
RSV/PBS
RSV/PX478 QD
RSV/PX478 QAD
Absolute Cell Count CD4/CD62L+/CD44-
Days Post-infection
B)
Absolute Cell Count CD4/CD62L-/CD44+
Days Post-infection
C)
Absolute Cell Count CD4/CD69+
Days Post-infection
D)
Absolute Cell Count CD4/FOXp3+
Days Post-infection
E)
Absolute Cell Count CD8/CD62L+/CD44-
Days Post-infection
F)
Absolute Cell Count CD8/CD62L-/CD44+
Days Post-infection
G)
Absolute Cell Count CD8/CD69+
Days Post-infection

Fig 3. *Assessment of $CD4^+$ and $CD8^+$ T-cells following HIF-1α inhibition during RSV infection.* At days 4 and 7 p.i., whole lung tissues were collected from the respective groups. Single cell suspension was prepared, stained with live/dead cell dye and fluorochrome-conjugated antibodies, and acquired by flow cytometry. Data were analyzed for (A) $CD4^+$ naive cells, (B) $CD4^+$ effector cells, (C) active $CD4^+$ cells, (D) $CD4^+$ Treg cells, (E) $CD8^+$ naive cells, (F) $CD8^+$ effector cells, and (G) active $CD8^+$ cells. Data are pooled from two independent experiments ($n \leq 10$ mice/group). Data are expressed as mean ± SEM. Significant results were determined by two-way ANOVA (* $p \leq 0.05$, ** $p \leq 0.01$, *** $p \leq 0.001$, **** $p \leq 0.0001$).

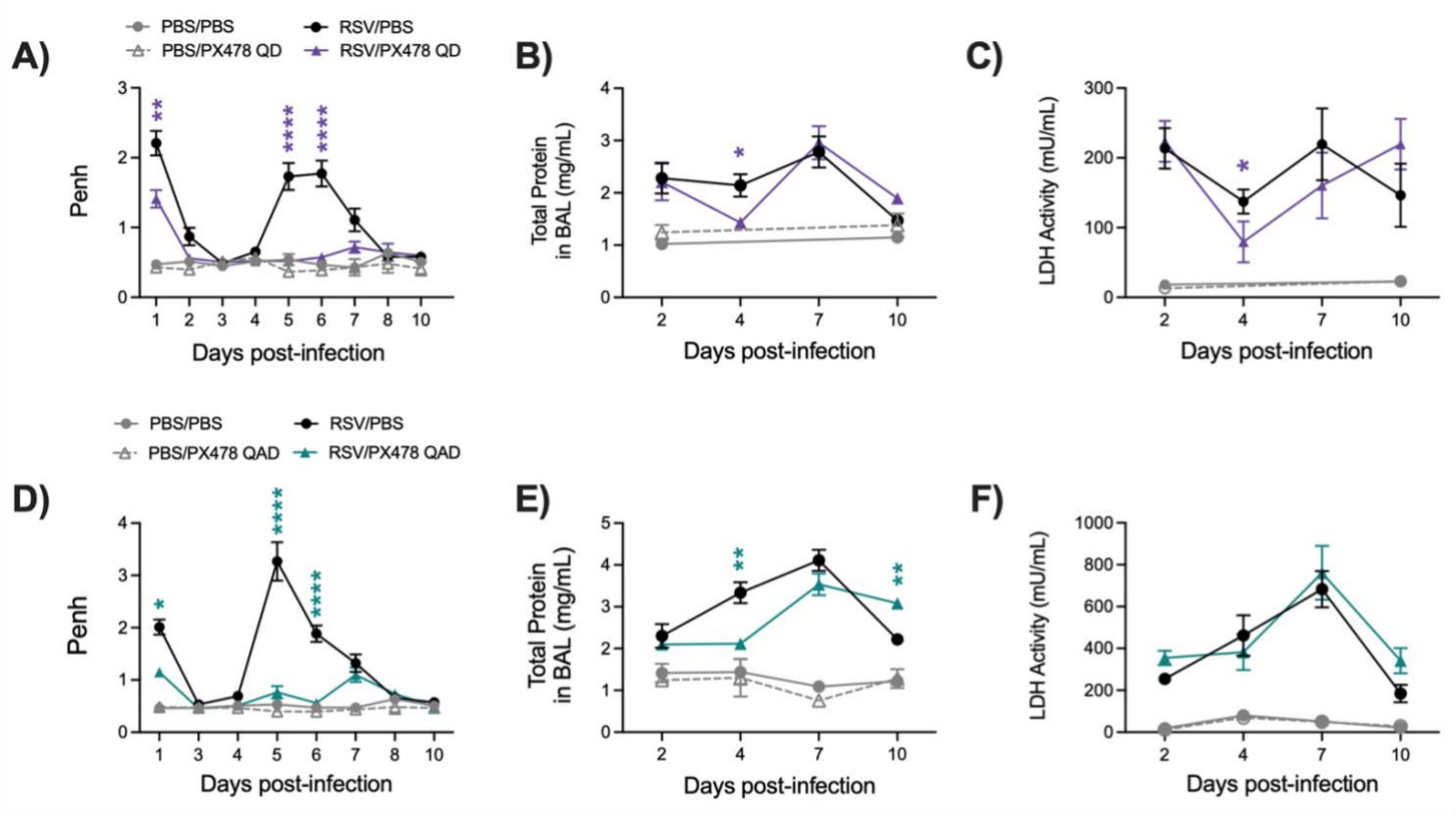

Fig 4. *Assessment of airway function following HIF-1α inhibition during RSV infection.* Airway function was determined in mice that received PX478 either (A-C) every 24 h or (D-F) every 48 h over the 10-day infection period. (A, D) Bronchoconstriction, represented by baseline Penh, was measured by plethysmography. Using BAL fluid collected at days 2, 4, 7, or 10 p.i., (B, E) total protein and (C, F) LDH were measured. For bronchoconstriction, data are pooled from three independent experiments ($n \leq 60$ mice/group). For total protein and LDH, data are pooled from two independent experiments ($n \leq 10$ mice/group). Data are expressed as mean ± SEM. Significant results were determined by mixed-effects analysis (* $p \leq 0.05$, ** $p \leq 0.01$, **** $p \leq 0.0001$).

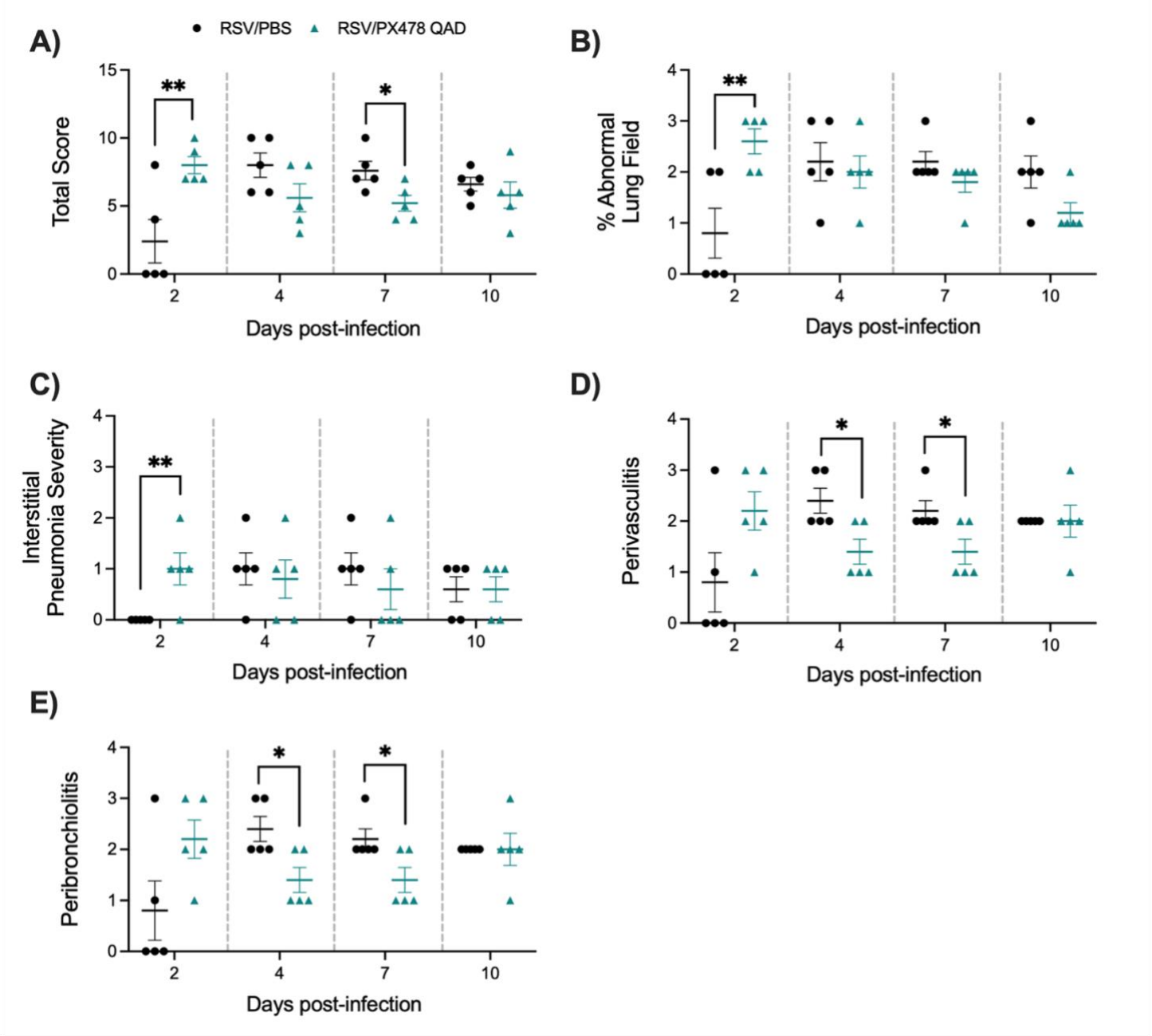
A)
RSV/PBS
RSV/PX478 QAD
Total Score
Days post-infection
B)
% Abnormal Lung Field
Days post-infection
C)
Interstitial Pneumonia Severity
Days post-infection
D)
Perivasculitis
Days post-infection
E)
Peribronchiolitis
Days post-infection

Fig 5. *Histopathological scoring of lung tissue following HIF-1α inhibition during RSV infection.* At days 2, 4, 7, and 10 p.i., the left lung was collected from mice that had received PBS or PX478 every 48 h and subjected to FFPE. Cuts of lung tissue were stained with H&E and the (A) total score was calculated, consisting of scores for (B) the percent abnormal lung field, (C) interstitial pneumonia, (D) perivasculitis, and (E) peribronchiolitis. Data are representative of one independent experiment (n = 5 mice/group). Data are expressed as mean ± SEM. Significant results were determined by student's t-test (* $p \leq 0.05$, ** $p \leq 0.01$).

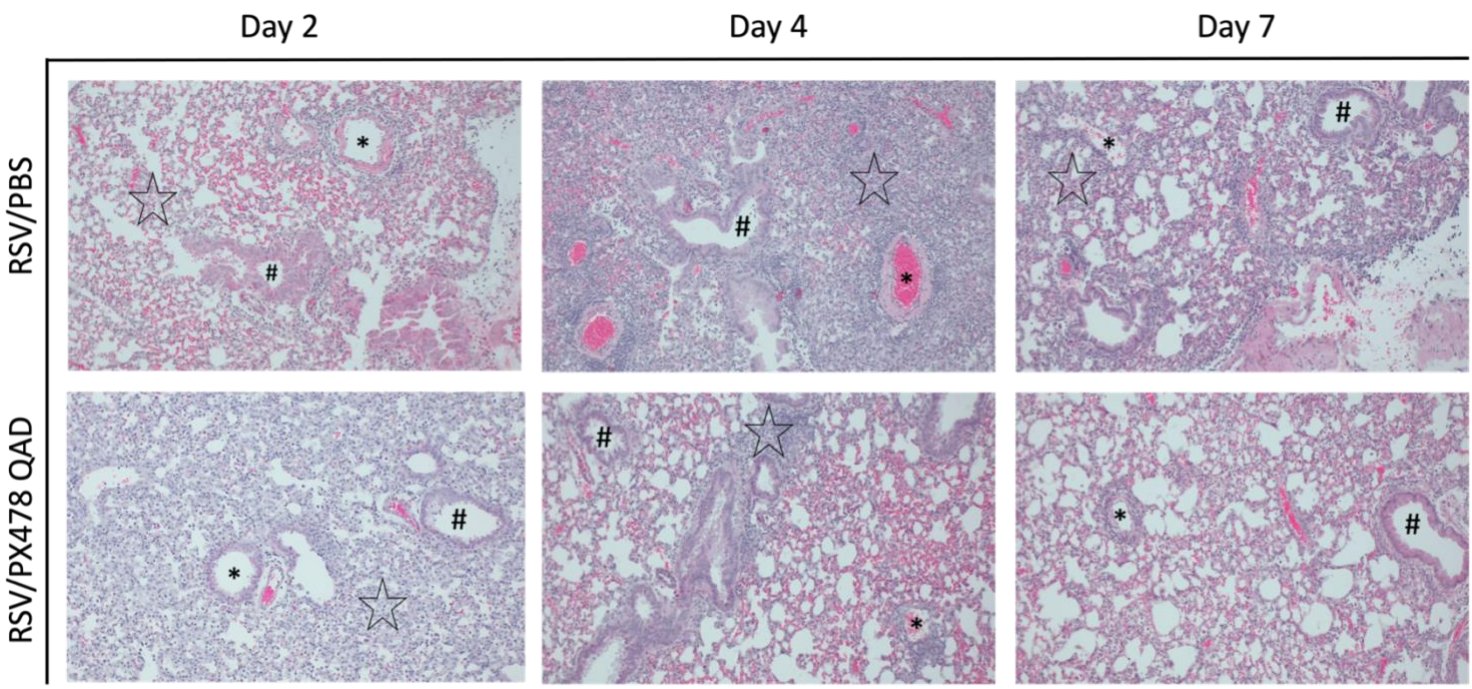

Fig 6. *Histopathological imaging of lung tissue following HIF-1α inhibition during RSV infection.* At days 2, 4, 7, and 10 p.i., the left lung was collected from mice that had received PBS or PX478 every 48 h and subjected to FFPE. Cuts of lung tissue were stained with H&E and observed under a microscope at 10X magnification. Perivasculitis is indicated by an asterisk. Peribronchiolitis is indicated by the hash sign. Interstitial pneumonia is indicated by the black star. No interstitial pneumonia present in RSV/PX478 QAD on day 7. Representative images are shown here (n = 5 mice/group).

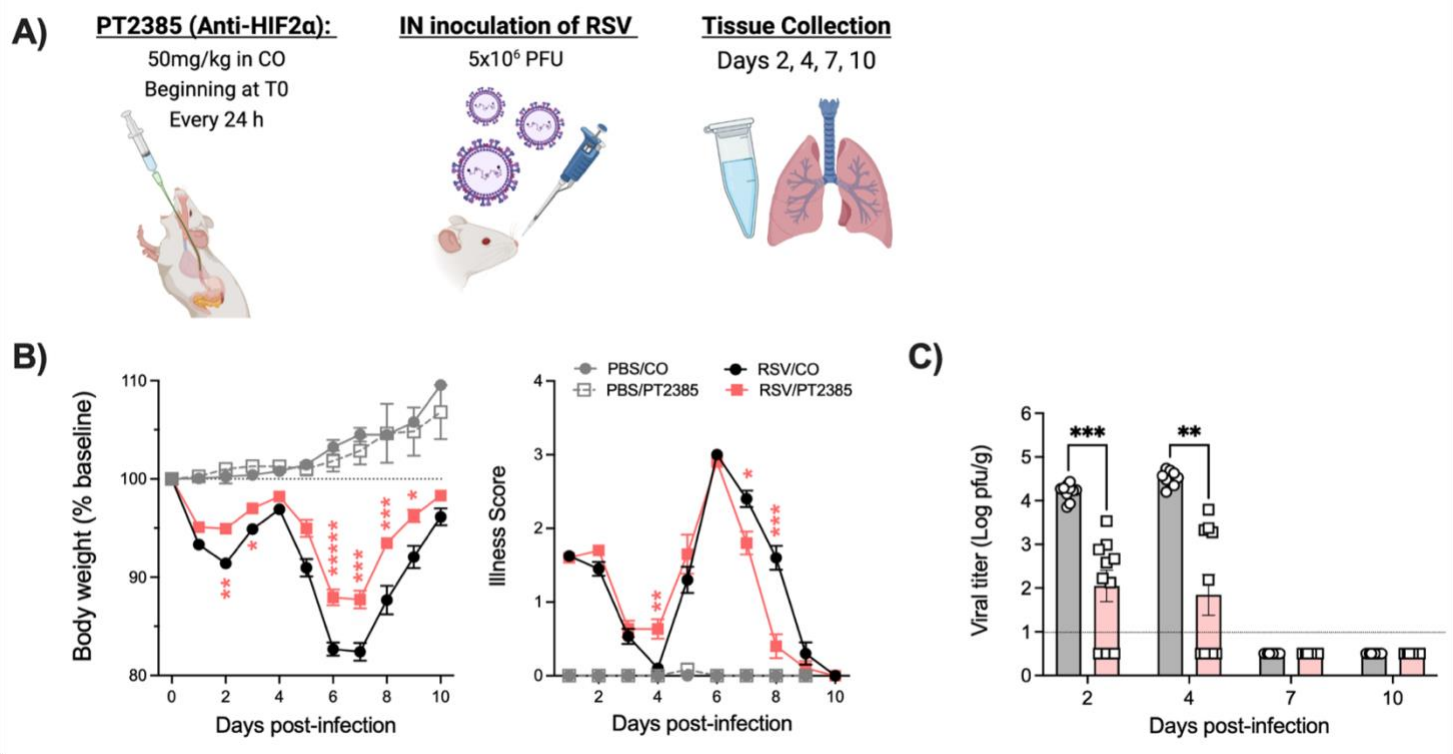

Fig 7. *Assessment of clinical disease and viral replication following HIF-2α inhibition during RSV infection.* (A) The experimental design for Figures 7-11. Detailed descriptions can be found in the methods section. Following treatment with PT2385 and RSV infection, mice were monitored daily for changes in (B) bodyweight loss and illness score. At days 2, 4, 7, and 10 p.i., the right lung was collected for assessment of (C) viral replication by plaque assay. For clinical disease, data are pooled from four independent experiments ($n \leq 70$ mice/group). For viral replication, data are pooled from two independent experiments ($n = 10$ mice/group). Data are expressed as mean ± SEM. Significant results were determined by two-way ANOVA or mixed effects analysis (* $p \leq 0.05$, ** $p \leq 0.01$, *** $p \leq 0.001$, **** $p \leq 0.0001$).

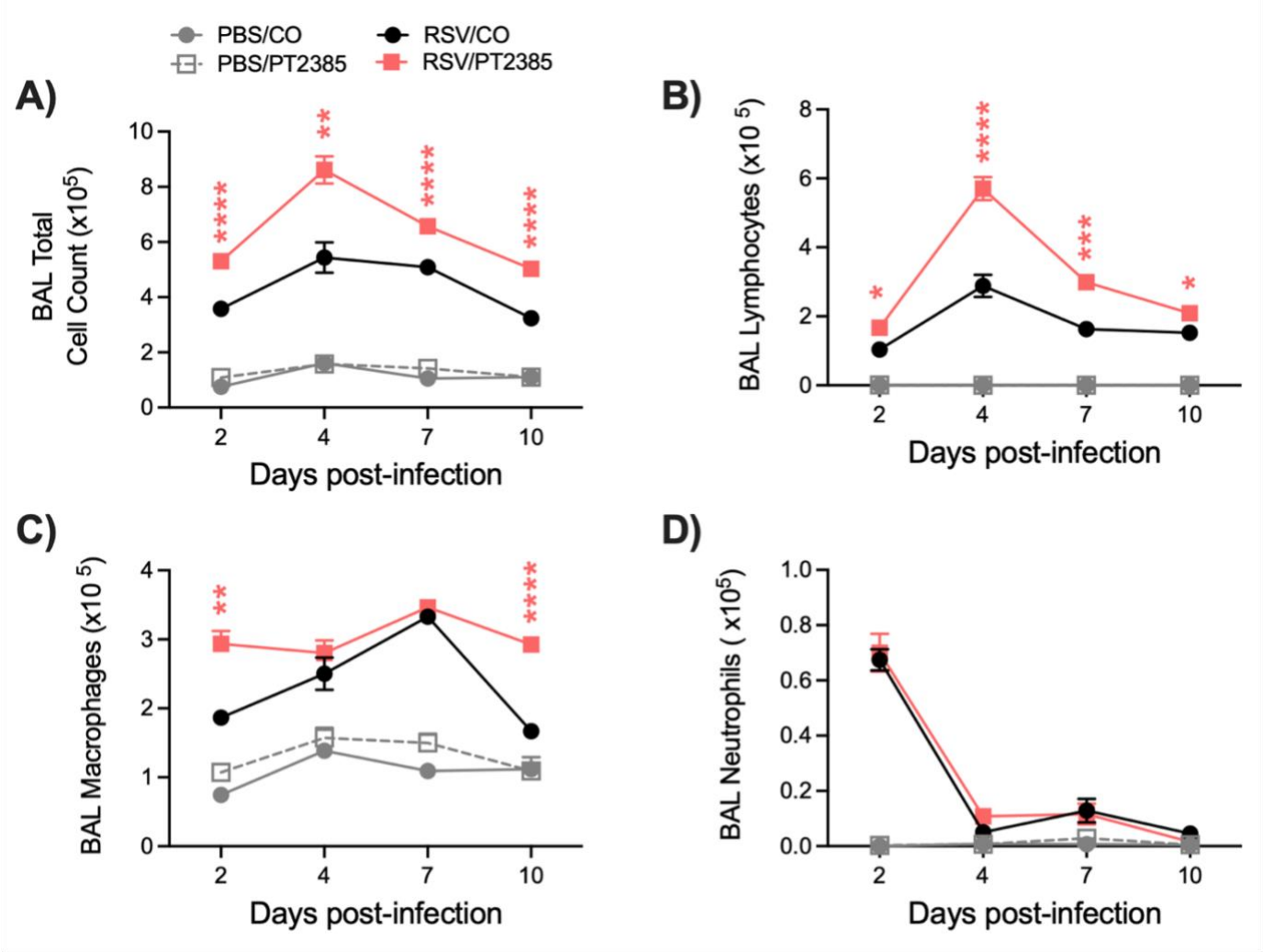

Fig 8. *Differential cell count of the BAL fluid following HIF-2α inhibition during RSV infection.* At days 2, 4, 7, and 10 p.i., BAL fluid was collected and used to obtain (A) total cell counts, as well as differential cell counts consisting of (B) lymphocytes, (C) macrophages, and (D) neutrophils. Data are pooled from two independent experiments (n ≤ 15 mice/group). Data are expressed as mean ± SEM. Significant results were determined by mixed-effects analysis (* $p \leq 0.05$, ** $p \leq 0.01$, *** $p \leq 0.001$, **** $p \leq 0.0001$).

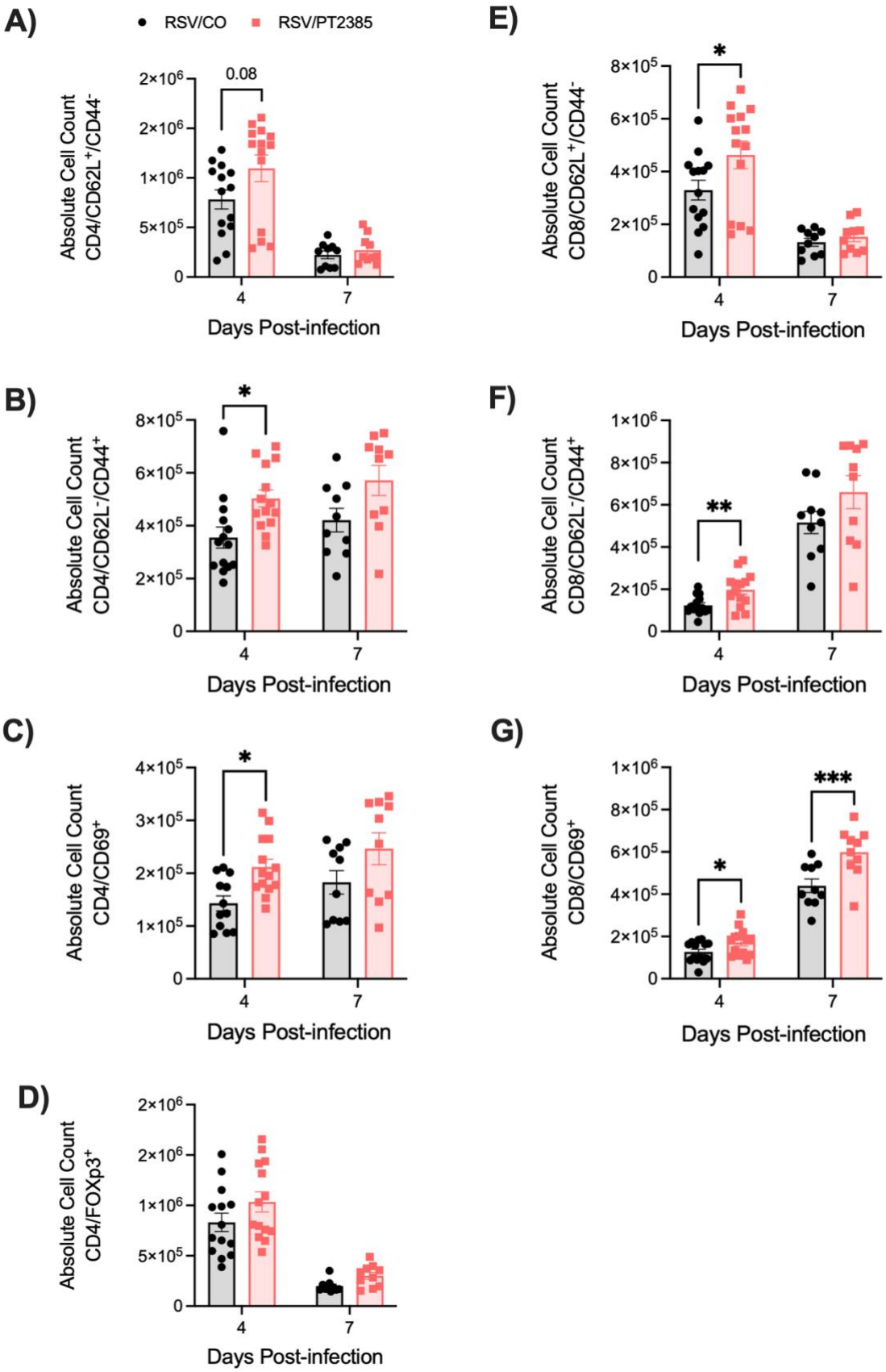
A)
RSV/CO
RSV/PT2385
0.08
Absolute Cell Count CD4/CD62L+/CD44-
Days Post-infection
B)
*
Absolute Cell Count CD4/CD62L-/CD44+
Days Post-infection
C)
*
Absolute Cell Count CD4/CD69+
Days Post-infection
D)
Absolute Cell Count CD4/FOXp3+
Days Post-infection
E)
*
Absolute Cell Count CD8/CD62L+/CD44-
Days Post-infection
F)
**
Absolute Cell Count CD8/CD62L-/CD44+
Days Post-infection
G)
*
***
Absolute Cell Count CD8/CD69+
Days Post-infection

<u>Fig 9.</u> *Assessment of CD4$^+$ and CD8$^+$ T-cells following HIF-2α inhibition during RSV infection.* At days 4 and 7 p.i., whole lung tissues were collected from the respective groups. Single cell suspension was prepared, stained with live/dead cell dye and fluorochrome-conjugated antibodies, and acquired by flow cytometry. Data were analyzed for of (A) CD4$^+$ naive cells, (B) CD4$^+$ effector cells, (C) active CD4$^+$ cells, (D) CD4$^+$ Treg cells, (E) CD8$^+$ naive cells, (F) CD8$^+$ effector cells, and (G) active CD8$^+$ cells. Data are pooled from three independent experiments for day 4 (n $\leq$ 15 mice/group) and two independent experiments for day 7 (n = 10 mice/group). Data are expressed as mean ± SEM. Significant results were determined by a two-way ANOVA or mixed-effects analysis (* $p \leq 0.05$, ** $p \leq 0.01$, *** $p \leq 0.001$).

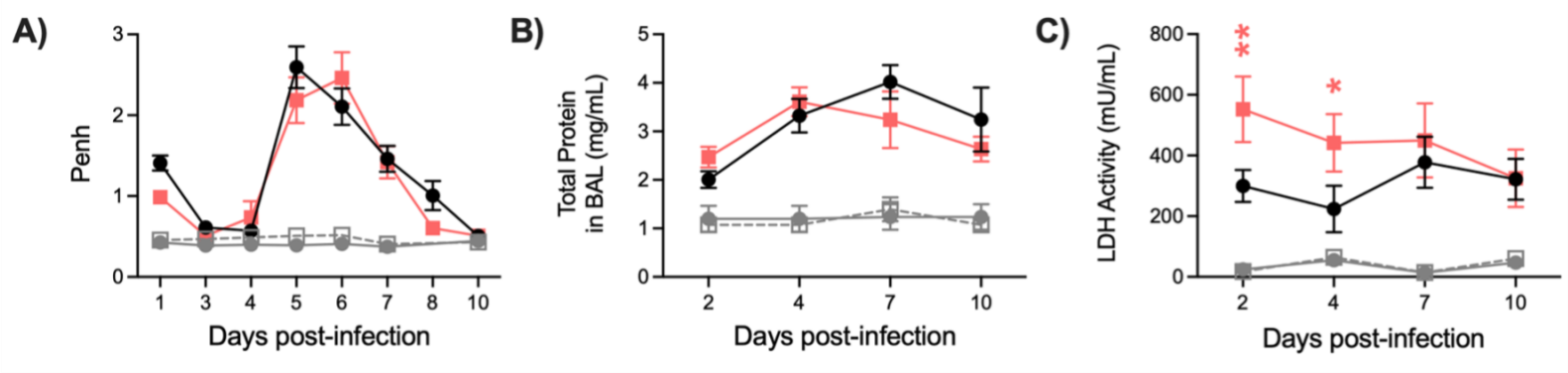

Fig 10. *Assessment of airway function following HIF-2α inhibition during RSV infection.* (A) Bronchoconstriction, represented by baseline Penh, was measured by plethysmography (Buxco Electronics Inc, Sharon, CT, USA). Using BAL fluid collected at days 2, 4, 7, and 10 p.i., (B) total protein and (C) LDH were measured. For bronchoconstriction, data are pooled from three independent experiments ($n \leq 25$ mice/group). For total protein and LDH, data are pooled from two independent experiments ($n \leq 10$ mice/group). Data are expressed as mean ± SEM. Significant results were determined by mixed-effects analysis (* $p \leq 0.05$, ** $p \leq 0.01$).

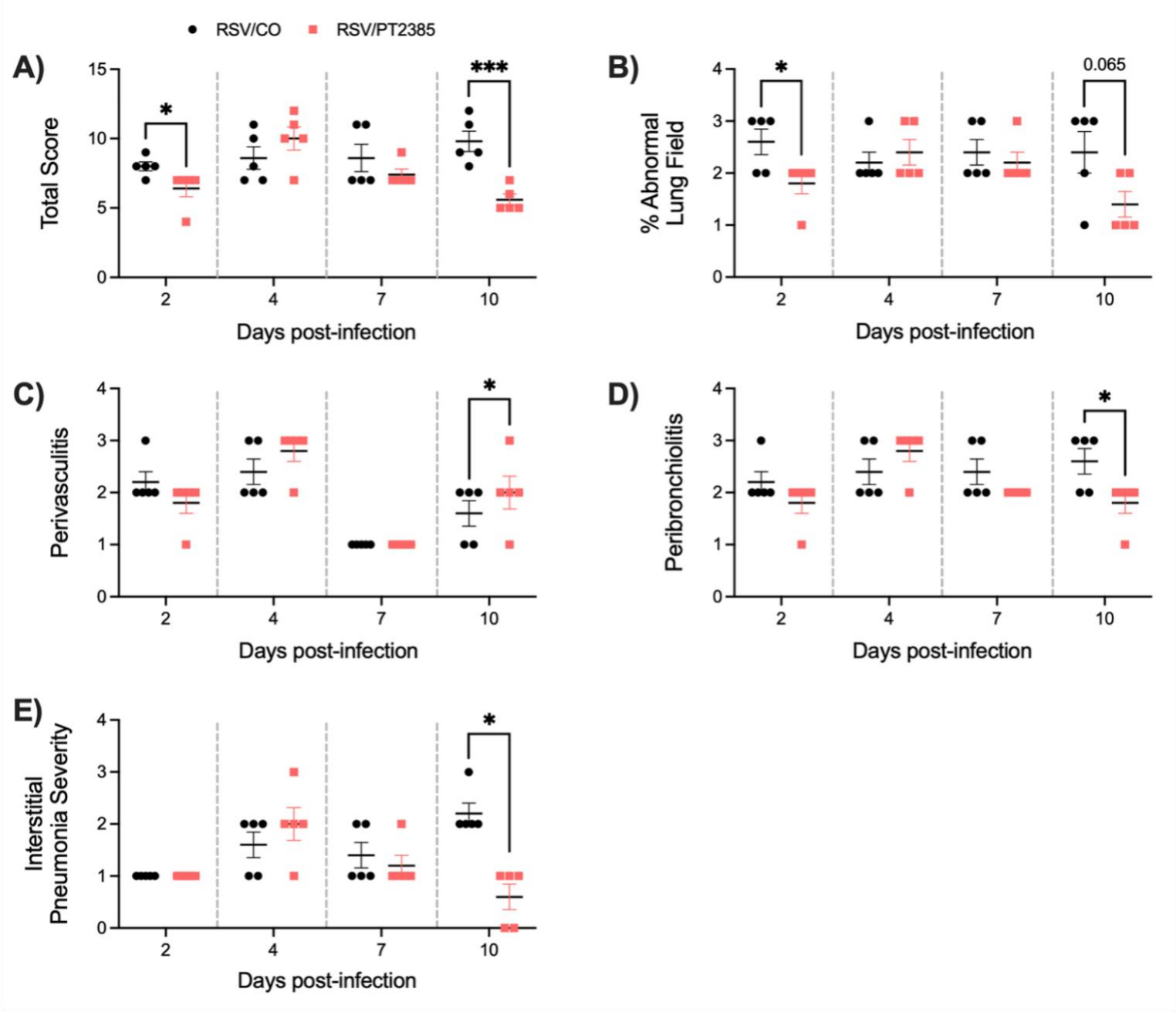
RSV/CO
RSV/PT2385
A)
Total Score
Days post-infection
B)
% Abnormal Lung Field
0.065
C)
Perivasculitis
D)
Peribronchiolitis
E)
Interstitial Pneumonia Severity

Fig 11. *Histopathological scoring of lung tissue following HIF-2α inhibition during RSV infection.* At days 2, 4, 7, and 10 p.i., the left lung was collected from mice that had received PBS or PT2385 and subjected to FFPE. Cuts of lung tissue were stained with H&E and the (A) total score was calculated, consisting of scores for (B) the percent abnormal lung field, (C) perivasculitis, (D) peribronchiolitis, and (E) interstitial pneumonia. Data are representative of one independent experiment (n = 5 mice/group). Data are expressed as mean ± SEM. Significant results were determined by student's t-test (* $p \leq 0.05$, *** $p \leq 0.001$).

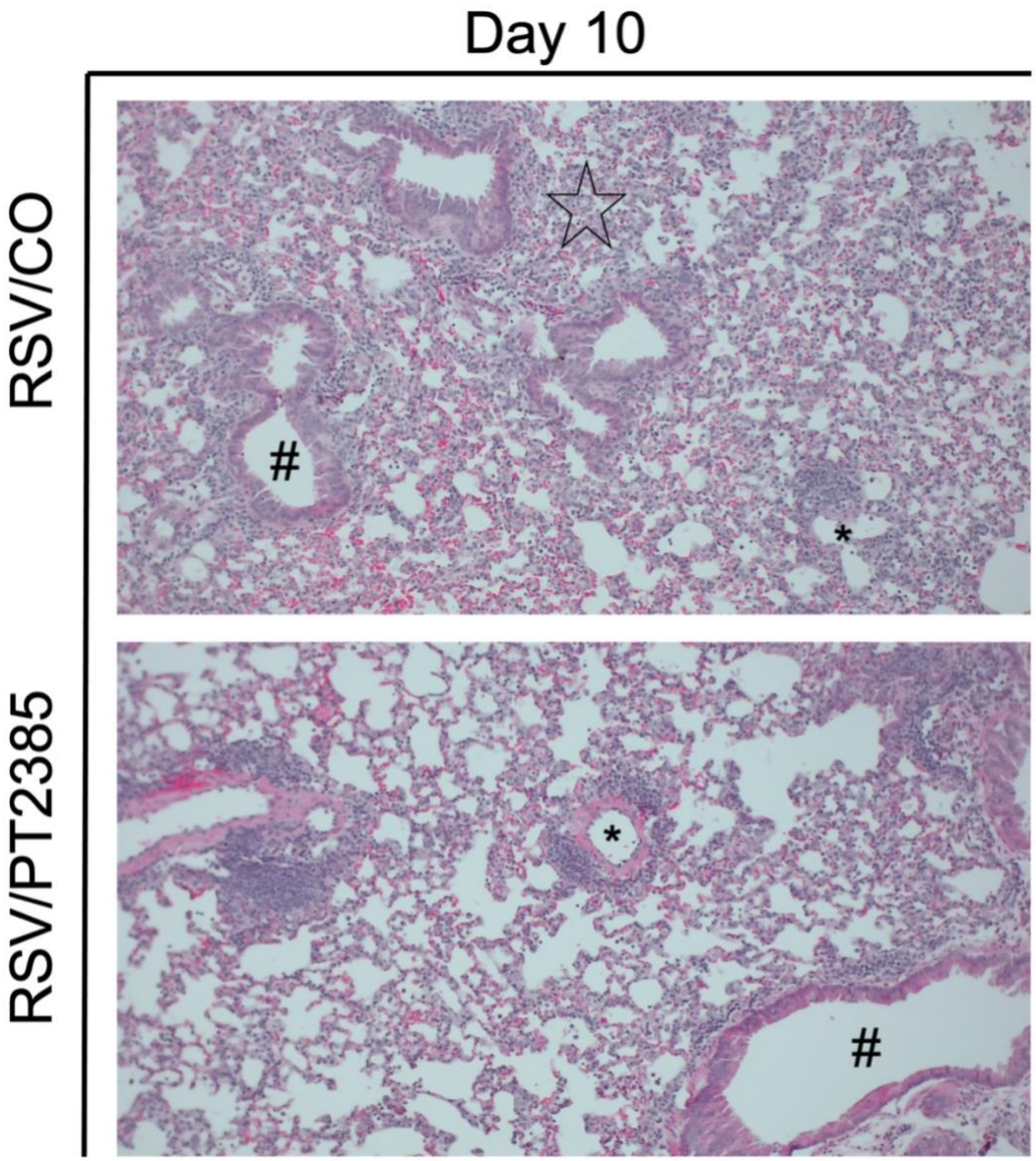

Fig 12. *Histopathological images of lung tissue following HIF-2a inhibition during RSV infection.* At days 2, 4, 7, and 10 p.i., the left lung was collected from mice that had received PBS or PT2385 and subjected to FFPE. Cuts of lung tissue were stained with H&E and observed under a microscope at 10X magnification. Perivasculitis is indicated by an asterisk. Peribronchiolitis is indicated by the hash symbol. Interstitial pneumonia is indicated by the black star. No interstitial pneumonia present in RSV/PT2385. Representative images are shown here (n = 5 mice/group).

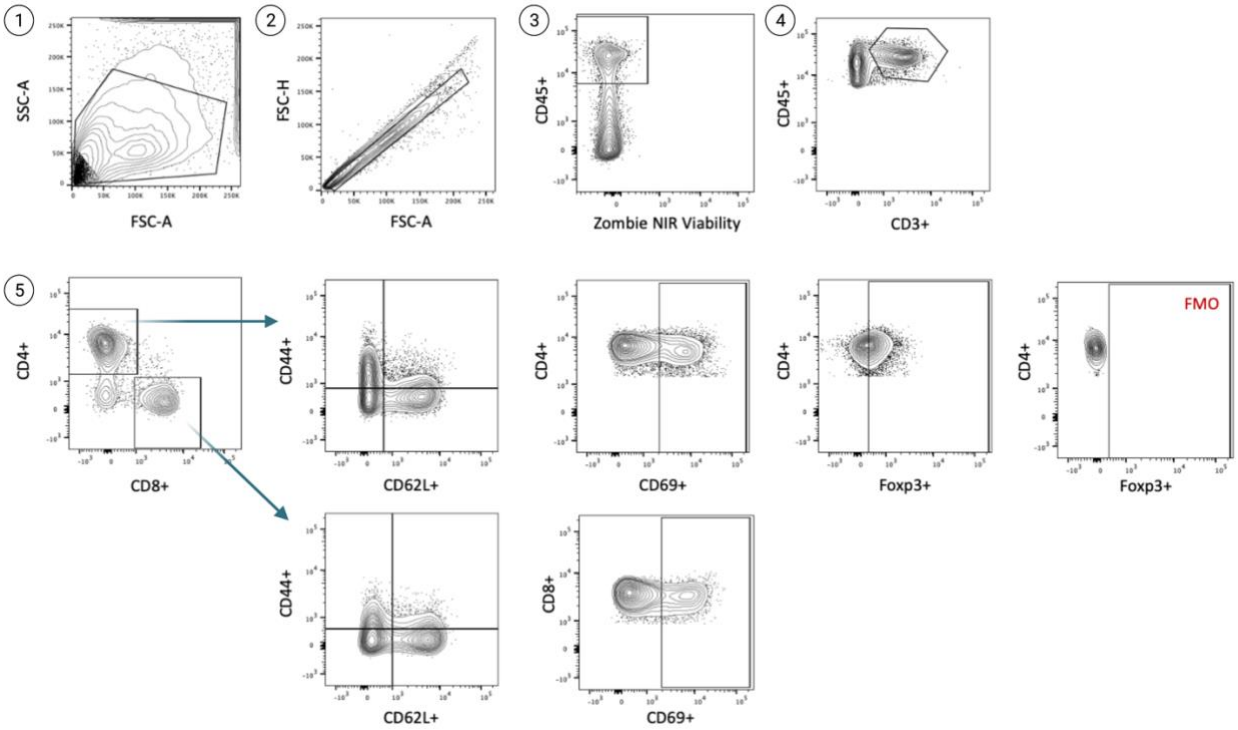

Fig S1. *Schematic for analysis of CD4+ and CD8+ T-cells by flow cytometry.* At days 4 and 7 p.i., whole lung tissue was collected from the respective groups. Single cell suspension was prepared, stained with live/dead cell dye and fluorochrome-conjugated antibodies, followed by flow cytometric analysis. T cells were gated on $CD45^{+}CD3^{+}$ first, then further gated on $CD4^{+}$ and $CD8^{+}$ subpopulations. Naïve and effector T cells were gated on $CD44^{-}CD62L^{+}$ and $CD44^{+}CD62L^{-}$ respectively. CD69 was used as an early activation marker of T cells. Tregs were defined as $CD45^{+}CD3^{+}CD4^{+}Foxp3^{+}$ and gated according to an FMO control.

Materials and Methods:

Ethics statement: All care and procedures involving mice in this study were completed in accordance with the recommendations in the *Guide for the Care and Use of Laboratory Animals* of the National Institutes of Health and the UTMB institutional guidelines for animal care. The Institutional Animal Care and Use Committee (IACUC) of UTMB approved these animal studies under protocol 9001002.

Animal Experiments: Female, 8 to 10-week-old BALB/c mice were purchased from Envigo (Indianapolis, IN, USA). Shortly before infection, mice received either PX478 or PT2385 by oral gavage at a dose of 20 or 50 mg/kg, respectively. PX489 was prepared in PBS and PT2385 was prepared in 10% DMSO + 90% Corn Oil (CO). The mechanism of action for each compound are described here [55,56]. Treatment regimens listed below were based on previous literature in which PX478 or PT2385 were used in non-infectious animal models as well as experimental dose testing. We originally chose a continuous treatment over the course of the disease period given the dual role of HIFs in regulating both acute infection and tissue recovery. For anti-HIF1α, PX478 treated mice were separated into three groups. The first received PBS as the control group. The second received PX478 every 24 h for 10 days (PXQD). The third group received PX478 every 48 h for 10 days (PXQAD). For anti-HIF2α, mice received either CO or PT2385 every 24 h for 10 days. Within 15 minutes of the first treatment, mice were anesthetized and intranasally (IN) inoculated with 50μL of either PBS or RSV Long Strain at a dose of $5x10^6$ PFU. All mice were monitored over the 10-day infection period for changes in bodyweight loss and illness score. Preparation of RSV Long Strain and descriptions of illness score criteria can be found here [57].

Bronchoalveolar lavage and viral replication: The BAL fluid was obtained as previously described [19]. A small aliquot was used to determine the total cell count and cellular differentiation of the BAL by cytospin analysis. The remaining BAL fluid was centrifuged, and the supernatants were collected and stored at -80C for future use. For viral replication, mice were euthanized, and the right lung was collected at days 2, 4, 7, and 10. Viral replication was evaluated by plaque assay as previously described [19].

Flow cytometry: At days 4 and 7 p.i., mice were euthanized and the whole lung was collected. The tissue was minced and digested with 10mg/mL DNase I (Sigma-Aldrich, St. Louis, MO, USA) and 50mg/mL collagenase IV (Worthington Biochemical, Lakewood, NJ, USA). The tissue was incubated at 37C for 30 minutes and then passed through a 70-μm cell strainer in RPMI 1640 medium + 10% FBS (CRPMI) and red blood cells were removed by using Red Blood Cell Lysis Buffer (Sigma-Aldrich, Burlington, MA, USA). TruStain FcX (Biolegend, San Diego, CA, USA) was first used to reduce non-specific binding, followed by Zombie NIR Viability dye. To assess CD4+ and CD8+ T-cell populations, the following fluorochrome-labeled antibodies were used: FITC-anti-CD45 (clone 30-F11), BV785-anti-CD3 (clone 17A2), AF 700-anti-CD4 (clone GK1.5), BV510-anti-CD8a (clone 53-6.7), PerCP/Cy5.5-anti-CD44 (clone IM7), BV605-anti-CD62L (clone MEL-14), and PE/Cy7-anti-CD69 (clone H1.2F3). Following surface antibody staining, cells were subjected to fixation and permeabilization overnight using the Foxp3/Transcription Factor Staining Buffer Set (Thermo Fisher Scientific, San Diego, CA, USA). The following day, BV421-anti-Foxp3 (clone MF-14) was added to assess Treg cell populations. All antibodies were purchased from Biolegend or Thermo Fisher Scientific and titrated prior to

use. Data were acquired on a BD FACSymphony A5 SE in the UTMB Flow Cytometry Core and analyzed using FlowJo software version 10.9.0 (BD Bioscience, Franklin Lakes, NJ, USA).

Assessment of airway function: Bronchoconstriction was evaluated by measuring Penh values in unrestrained mice using whole-body barometric plethysmography (Buxco, Troy, NY, USA) as previously described [58]. Total protein and LDH activity of the BAL were used to assess lung epithelial integrity and general cell death. Total protein was measuring using BioRad Total Protein Dye (Bio-Rad Laboratories, Hercules, CA, USA). LDH activity was measured using the Lactate Dehydrogenase Activity Assay Kit (Sigma-Aldrich, St. Louis, MO, USA).

Histopathology: At days 2, 4, 7, and 10 p.i., mice were euthanized, and the left lung was collected. The tissue was fixed in 10% neutral buffered formalin and subjected to paraffin embedding. Sections were cut and stained with H&E and evaluated by a board-certified pathologist with expertise in mouse lung (Y.L.J.-H). Assessment of the tissue was done as previously described [59].

Statistical analysis: Statistical analyses were performed using an ordinary two-way ANOVA followed by Tukey's multiple comparison test, a mixed-effects model followed by Geisser-Greenhouse correction, or an unpaired student's t-test (indicated in figure legends). These were done using GraphPad Prism 9.5.1 (GraphPad Software, Inc., San Diego, CA, USA). Results are expressed as mean ± SEM and $p \leq 0.05$ value was selected to indicate significance.

Acknowledgements: We would like to thank Vineet Menachery, Yuejin Liang, Casey Wright, and Xiaoyi Yuan for their thoughtful discussion. We would also like to thank the Texas A&M University Veterinary Medicine and Biomedical Sciences Research Histology Core Facility for their assistance with the tissue processing. Biorender.com was used to produce the experimental design summaries. DRM was supported by the McLaughlin Endowment Predoctoral Fellowship and the NIH Clinical and Translational Science Award NRSA (TL1) Training Core TL1TR001440. This research was additionally funded by an Institute for Human Infections and Immunity (IHII) Pilot Grant and by NIH grants AI62884 and AI175955.

References:

1. Shi, T.; McAllister, D.A.; O'Brien, K.L.; Simoes, E.A.F.; Madhi, S.A.; Gessner, B.D.; Polack, F.P.; Balsells, E.; Acacio, S.; Aguayo, C., et al. Global, regional, and national disease burden estimates of acute lower respiratory infections due to respiratory syncytial virus in young children in 2015: a systematic review and modelling study. *The Lancet* **2017**, *390*, 946-958, doi:https://doi.org/10.1016/S0140-6736(17)30938-8.
2. Altman, J.D.; Rouse, B.T. The Long-Awaited Respiratory Syncytial Virus Vaccine. *J Interferon Cytokine Res* **2023**, *43*, 285-286, doi:10.1089/jir.2023.0076.
3. Kampmann, B.; Madhi, S.A.; Munjal, I.; Simões, E.A.F.; Pahud, B.A.; Llapur, C.; Baker, J.; Pérez Marc, G.; Radley, D.; Shittu, E., et al. Bivalent Prefusion F Vaccine in Pregnancy to Prevent RSV Illness in Infants. *New England Journal of Medicine* **2023**, *388*, 1451-1464, doi:10.1056/NEJMoa2216480.
4. Papi, A.; Ison, M.G.; Langley, J.M.; Lee, D.-G.; Leroux-Roels, I.; Martinon-Torres, F.; Schwarz, T.F.; van Zyl-Smit, R.N.; Campora, L.; Dezutter, N., et al. Respiratory Syncytial Virus Prefusion F Protein Vaccine in Older Adults. *New England Journal of Medicine* **2023**, *388*, 595-608, doi:10.1056/NEJMoa2209604.
5. Thaker, S.K.; Ch'ng, J.; Christofk, H.R. Viral hijacking of cellular metabolism. *BMC Biology* **2019**, *17*, 59, doi:10.1186/s12915-019-0678-9.
6. Morris, D.R.; Qu, Y.; Agrawal, A.; Garofalo, R.P.; Casola, A. HIF-1α Modulates Core Metabolism and Virus Replication in Primary Airway Epithelial Cells Infected with Respiratory Syncytial Virus. *Viruses* **2020**, *12*, doi:10.3390/v12101088.
7. Brahimi-Horn, M.C.; Pouysségur, J. HIF at a glance. *Journal of cell science* **2009**, *122*, 1055-1057, doi:10.1242/jcs.035022.
8. Infantino, V.; Santarsiero, A.; Convertini, P.; Todisco, S.; Iacobazzi, V. Cancer Cell Metabolism in Hypoxia: Role of HIF-1 as Key Regulator and Therapeutic Target. *International journal of molecular sciences* **2021**, *22*, 5703.
9. Koh, M.Y.; Powis, G. Passing the baton: the HIF switch. *Trends in biochemical sciences* **2012**, *37*, 364-372, doi:10.1016/j.tibs.2012.06.004.
10. Zhang, P.; Yao, Q.; Lu, L.; Li, Y.; Chen, P.-J.; Duan, C. Hypoxia-Inducible Factor 3 Is an Oxygen-Dependent Transcription Activator and Regulates a Distinct Transcriptional Response to Hypoxia. *Cell reports* **2014**, *6*, 1110-1121, doi:https://doi.org/10.1016/j.celrep.2014.02.011.
11. Downes, N.L.; Laham-Karam, N.; Kaikkonen, M.U.; Yla-Herttuala, S. Differential but Complementary HIF1alpha and HIF2alpha Transcriptional Regulation. *Mol Ther* **2018**, *26*, 1735-1745, doi:10.1016/j.ymthe.2018.05.004.
12. Reyes, A.; Corrales, N.; Gálvez, N.M.S.; Bueno, S.M.; Kalergis, A.M.; González, P.A. Contribution of hypoxia inducible factor-1 during viral infections. *Virulence* **2020**, *11*, 1482-1500, doi:10.1080/21505594.2020.1836904.
13. Huang, R.; Huestis, M.; Gan, E.S.; Ooi, E.E.; Ohh, M. Hypoxia and viral infectious diseases. *JCI Insight* **2021**, *6*, doi:10.1172/jci.insight.147190.
14. Semenza, G.L. Pharmacologic Targeting of Hypoxia-Inducible Factors. *Annual Review of Pharmacology and Toxicology* **2019**, *59*, 379-403, doi:10.1146/annurev-pharmtox-010818-021637.
15. Reyes, A.; Duarte, L.F.; Farías, M.A.; Tognarelli, E.; Kalergis, A.M.; Bueno, S.M.; González, P.A. Impact of Hypoxia over Human Viral Infections and Key Cellular

Processes. *International journal of molecular sciences* **2021**, *22*, doi:10.3390/ijms22157954.

16. Russell, C.D.; Unger, S.A.; Walton, M.; Schwarze, J. The Human Immune Response to Respiratory Syncytial Virus Infection. **2017**, *30*, 481-502, doi:10.1128/CMR.00090-16 %J Clinical Microbiology Reviews.
17. De, C.; Pickles, R.J.; Yao, W.; Liao, B.; Boone, A.; Choi, M.; Battaglia, D.M.; Askin, F.B.; Whitmire, J.K.; Silvestri, G., et al. Human T cells efficiently control RSV infection. *JCI Insight* **2023**, *8*, doi:10.1172/jci.insight.168110.
18. McGinley, J.; Thwaites, R.; Brebner, W.; Greenan-Barrett, L.; Aerssens, J.; Öner, D.; Bont, L.; Wildenbeest, J.; Martinón-Torres, F.; Nair, H., et al. A Systematic Review and Meta-analysis of Animal Studies Investigating the Relationship Between Serum Antibody, T Lymphocytes, and Respiratory Syncytial Virus Disease. *The Journal of Infectious Diseases* **2021**, *226*, S117-S129, doi:10.1093/infdis/jiab370.
19. Morris, D.R.; Ansar, M.; Ivanciuc, T.; Qu, Y.; Casola, A.; Garofalo, R.P. Selective Blockade of TNFR1 Improves Clinical Disease and Bronchoconstriction in Experimental RSV Infection. *Viruses* **2020**, *12*, doi:10.3390/v12101176.
20. Wicks, E.E.; Semenza, G.L. Hypoxia-inducible factors: cancer progression and clinical translation. *The Journal of clinical investigation* **2022**, *132*, doi:10.1172/JCI159839.
21. Lee, J.W.; Ko, J.; Ju, C.; Eltzschig, H.K. Hypoxia signaling in human diseases and therapeutic targets. *Experimental & Molecular Medicine* **2019**, *51*, 1-13, doi:10.1038/s12276-019-0235-1.
22. Jacoby, J.J.; Erez, B.; Korshunova, M.V.; Williams, R.R.; Furutani, K.; Takahashi, O.; Kirkpatrick, L.; Lippman, S.M.; Powis, G.; O'Reilly, M.S., et al. Treatment with HIF-1alpha antagonist PX-478 inhibits progression and spread of orthotopic human small cell lung cancer and lung adenocarcinoma in mice. *J Thorac Oncol* **2010**, *5*, 940-949, doi:10.1097/JTO.0b013e3181dc211f.
23. Xu, L.; Ishikawa, H.; Zhou, Y.; Kobayashi, T.; Shozu, M. Antitumor effect of the selective hypoxia-inducible factor-1 inhibitors echinomycin and PX-478 on uterine fibroids. *F S Sci* **2022**, *3*, 187-196, doi:10.1016/j.xfss.2022.01.005.
24. Welsh, S.; Williams, R.; Kirkpatrick, L.; Paine-Murrieta, G.; Powis, G. Antitumor activity and pharmacodynamic properties of PX-478, an inhibitor of hypoxia-inducible factor-1α. *Molecular cancer therapeutics* **2004**, *3*, 233-244, doi:10.1158/1535-7163.233.3.3.
25. Palayoor, S.T.; Mitchell, J.B.; Cerna, D.; DeGraff, W.; John-Aryankalayil, M.; Coleman, C.N. PX-478, an inhibitor of hypoxia-inducible factor-1α, enhances radiosensitivity of prostate carcinoma cells. *Int J Cancer* **2008**, *123*, 2430-2437, doi:https://doi.org/10.1002/ijc.23807.
26. Xu, K.; Zhan, Y.; Yuan, Z.; Qiu, Y.; Wang, H.; Fan, G.; Wang, J.; Li, W.; Cao, Y.; Shen, X., et al. Hypoxia Induces Drug Resistance in Colorectal Cancer through the HIF-1alpha/miR-338-5p/IL-6 Feedback Loop. *Mol Ther* **2019**, *27*, 1810-1824, doi:10.1016/j.ymthe.2019.05.017.
27. Abe, Y.; Mukudai, Y.; Kurihara, M.; Houri, A.; Chikuda, J.; Yaso, A.; Kato, K.; Shimane, T.; Shirota, T. Tumor protein D52 is upregulated in oral squamous carcinoma cells under hypoxia in a hypoxia-inducible-factor-independent manner and is involved in cell death resistance. *Cell & bioscience* **2021**, *11*, 122, doi:10.1186/s13578-021-00634-0.

28. Tibes, R.; Falchook, G.S.; Von Hoff, D.D.; Weiss, G.J.; Iyengar, T.; Kurzrock, R.; Pestano, L.; Lowe, A.M.; Herbst, R.S. Results from a phase I, dose-escalation study of PX-478, an orally available inhibitor of HIF-1α. *Journal of Clinical Oncology* **2010**, *28*, 3076-3076, doi:10.1200/jco.2010.28.15_suppl.3076.
29. Tibes, R.; Falchook, G.S.; Hoff, D.D.V.; Weiss, G.J.; Iyengar, T.; Kurzrock, R.; Pestano, L.; Lowe, A.M.; Herbst, R.S. Results from a phase I, dose-escalation study of PX-478, an orally available inhibitor of HIF-1α. *Journal of Clinical Oncology* **2010**, *28*, 3076-3076, doi:10.1200/jco.2010.28.15_suppl.3076.
30. Villa-Roel, N.; Ryu, K.; Gu, L.; Fernandez Esmerats, J.; Kang, D.-W.; Kumar, S.; Jo, H. Hypoxia inducible factor 1α inhibitor PX-478 reduces atherosclerosis in mice. *Atherosclerosis* **2022**, *344*, 20-30, doi:https://doi.org/10.1016/j.atherosclerosis.2022.01.002.
31. Sun, K.; Halberg, N.; Khan, M.; Magalang, U.J.; Scherer, P.E. Selective Inhibition of Hypoxia-Inducible Factor 1α Ameliorates Adipose Tissue Dysfunction. *Molecular and cellular biology* **2013**, *33*, 904-917, doi:10.1128/MCB.00951-12.
32. Ilegems, E.; Bryzgalova, G.; Correia, J.; Yesildag, B.; Berra, E.; Ruas, J.L.; Pereira, T.S.; Berggren, P.-O. HIF-1a inhibitor PX-478 preserves pancreatic beta cell function in diabetes. *Science translational medicine* **2022**, *14*, eaba9112, doi:doi:10.1126/scitranslmed.aba9112.
33. Taylor, C.T.; Scholz, C.C. The effect of HIF on metabolism and immunity. *Nature Reviews Nephrology* **2022**, *18*, 573-587, doi:10.1038/s41581-022-00587-8.
34. Martín-Vicente, M.; González-Riaño, C.; Barbas, C.; Jiménez-Sousa, M.; Brochado-Kith, O.; Resino, S.; Martínez, I. Metabolic changes during respiratory syncytial virus infection of epithelial cells. *PloS one* **2020**, *15*, e0230844, doi:10.1371/journal.pone.0230844.
35. Connelly, A.R.; Jeong, B.M.; Coden, M.E.; Cao, J.Y.; Chirkova, T.; Rosas-Salazar, C.; Cephus, J.Y.; Anderson, L.J.; Newcomb, D.C.; Hartert, T.V., et al. Metabolic Reprogramming of Nasal Airway Epithelial Cells Following Infant Respiratory Syncytial Virus Infection. *Viruses* **2021**, *13*, doi:10.3390/v13102055.
36. Li, M.; Li, J.; Zeng, R.; Yang, J.; Liu, J.; Zhang, Z.; Song, X.; Yao, Z.; Ma, C.; Li, W., et al. Respiratory Syncytial Virus Replication Is Promoted by Autophagy-Mediated Inhibition of Apoptosis. *Journal of virology* **2018**, *92*, 10.1128/jvi.02193-02117, doi:doi:10.1128/jvi.02193-17.
37. Chiok, K.; Pokharel, S.M.; Mohanty, I.; Miller, L.G.; Gao, S.J.; Haas, A.L.; Tran, K.C.; Teng, M.N.; Bose, S. Human Respiratory Syncytial Virus NS2 Protein Induces Autophagy by Modulating Beclin1 Protein Stabilization and ISGylation. *mBio* **2022**, *13*, e0352821, doi:10.1128/mbio.03528-21.
38. Shuchi, S.; Ratho, R.K.; Mohi, G.K.; Kumar Angurana, S.; Sarkar, S.; Jangra, I. Modulation of autophagy and mTOR signaling pathway genes in respiratory epithelium by respiratory syncytial virus (RSV) in children suffering from acute lower respiratory tract infections. *Journal of Medical Virology* **2023**, *95*, e28666, doi:https://doi.org/10.1002/jmv.28666.
39. Zhang, H.; Bosch-Marce, M.; Shimoda, L.A.; Tan, Y.S.; Baek, J.H.; Wesley, J.B.; Gonzalez, F.J.; Semenza, G.L. Mitochondrial autophagy is an HIF-1-dependent adaptive metabolic response to hypoxia. *The Journal of biological chemistry* **2008**, *283*, 10892-10903, doi:10.1074/jbc.M800102200.

40. Zhou, J.; Li, C.; Yao, W.; Alsiddig, M.C.; Huo, L.; Liu, H.; Miao, Y.-L. Hypoxia-inducible factor-1α-dependent autophagy plays a role in glycolysis switch in mouse granulosa cells†. *Biology of Reproduction* **2018**, *99*, 308-318, doi:10.1093/biolre/ioy061.
41. Bhat, R.; Farrag, M.A.; Almajhdi, F.N. Double-edged role of natural killer cells during RSV infection. *International reviews of immunology* **2020**, *39*, 233-244, doi:10.1080/08830185.2020.1770748.
42. Bergeron, H.C.; Tripp, R.A. Immunopathology of RSV: An Updated Review. *Viruses* **2021**, *13*, 2478.
43. Luckheeram, R.V.; Zhou, R.; Verma, A.D.; Xia, B. $CD4^+$T cells: differentiation and functions. *Clin Dev Immunol* **2012**, *2012*, 925135, doi:10.1155/2012/925135.
44. Schmidt, M.E.; Varga, S.M. Cytokines and CD8 T cell immunity during respiratory syncytial virus infection. *Cytokine* **2020**, *133*, 154481, doi:10.1016/j.cyto.2018.07.012.
45. McGettrick, A.F.; O'Neill, L.A.J. The Role of HIF in Immunity and Inflammation. *Cell metabolism* **2020**, *32*, 524-536, doi:10.1016/j.cmet.2020.08.002.
46. Hsu, T.-S.; Lin, Y.-L.; Wang, Y.-A.; Mo, S.-T.; Chi, P.-Y.; Lai, A.C.-Y.; Pan, H.-Y.; Chang, Y.-J.; Lai, M.-Z. HIF-2α is indispensable for regulatory T cell function. *Nature communications* **2020**, *11*, 5005, doi:10.1038/s41467-020-18731-y.
47. Ajouaou, Y.; Azouz, A.; Taquin, A.; Denanglaire, S.; Hussein, H.; Krayem, M.; Andris, F.; Moser, M.; Goriely, S.; Leo, O. The oxygen sensor prolyl hydroxylase domain 2 regulates the in vivo suppressive capacity of regulatory T cells. *eLife* **2022**, *11*, e70555, doi:10.7554/eLife.70555.
48. Ahmad, T.; Kumar, M.; Mabalirajan, U.; Pattnaik, B.; Aggarwal, S.; Singh, R.; Singh, S.; Mukerji, M.; Ghosh, B.; Agrawal, A. Hypoxia response in asthma: differential modulation on inflammation and epithelial injury. *American journal of respiratory cell and molecular biology* **2012**, *47*, 1-10, doi:10.1165/rcmb.2011-0203OC.
49. Dewitz, C.; McEachern, E.; Shin, S.; Akong, K.; Nagle, D.G.; Broide, D.H.; Akuthota, P.; Crotty Alexander, L.E. Hypoxia-inducible factor-1α inhibition modulates airway hyperresponsiveness and nitric oxide levels in a BALB/c mouse model of asthma. *Clinical Immunology* **2017**, *176*, 94-99, doi:https://doi.org/10.1016/j.clim.2017.01.002.
50. Pan, S.; Conaway, S., Jr.; Deshpande, D.A. Mitochondrial regulation of airway smooth muscle functions in health and pulmonary diseases. *Archives of biochemistry and biophysics* **2019**, *663*, 109-119, doi:10.1016/j.abb.2019.01.002.
51. Bartman, C.M.; Matveyenko, A.; Pabelick, C.; Prakash, Y.S. Cellular clocks in hyperoxia effects on [Ca2+]i regulation in developing human airway smooth muscle. *American Journal of Physiology-Lung Cellular and Molecular Physiology* **2021**, *320*, L451-L466, doi:10.1152/ajplung.00406.2020.
52. Evans, C.E. Hypoxia-Inducible Factor Signaling in Inflammatory Lung Injury and Repair. *Cells* **2022**, *11*, doi:10.3390/cells11020183.
53. Hosakote, Y.M.; Liu, T.; Castro, S.M.; Garofalo, R.P.; Casola, A. Respiratory syncytial virus induces oxidative stress by modulating antioxidant enzymes. *American journal of respiratory cell and molecular biology* **2009**, *41*, 348-357, doi:10.1165/rcmb.2008-0330OC.
54. Stegen, S.; van Gastel, N.; Eelen, G.; Ghesquiere, B.; D'Anna, F.; Thienpont, B.; Goveia, J.; Torrekens, S.; Van Looveren, R.; Luyten, F.P., et al. HIF-1alpha Promotes Glutamine-Mediated Redox Homeostasis and Glycogen-Dependent Bioenergetics to Support

Postimplantation Bone Cell Survival. *Cell metabolism* **2016**, *23*, 265-279, doi:10.1016/j.cmet.2016.01.002.

55. Koh, M.Y.; Spivak-Kroizman, T.; Venturini, S.; Welsh, S.; Williams, R.R.; Kirkpatrick, D.L.; Powis, G. Molecular mechanisms for the activity of PX-478, an antitumor inhibitor of the hypoxia-inducible factor-1α. *Molecular cancer therapeutics* **2008**, *7*, 90, doi:10.1158/1535-7163.MCT-07-0463.
56. Wu, D.; Su, X.; Lu, J.; Li, S.; Hood, B.L.; Vasile, S.; Potluri, N.; Diao, X.; Kim, Y.; Khorasanizadeh, S., et al. Bidirectional modulation of HIF-2 activity through chemical ligands. *Nature Chemical Biology* **2019**, *15*, 367-376, doi:10.1038/s41589-019-0234-5.
57. Ivanciuc, T.; Patrikeev, I.; Qu, Y.; Motamedi, M.; Jones-Hall, Y.; Casola, A.; Garofalo, R.P. Micro-CT Features of Lung Consolidation, Collagen Deposition and Inflammation in Experimental RSV Infection Are Aggravated in the Absence of Nrf2. *Viruses* **2023**, *15*, doi:10.3390/v15051191.
58. Morris, D.; Ansar, M.; Speshock, J.; Ivanciuc, T.; Qu, Y.; Casola, A.; Garofalo, R. Antiviral and Immunomodulatory Activity of Silver Nanoparticles in Experimental RSV Infection. *Viruses* **2019**, *11*, doi:10.3390/v11080732.
59. Qu, Y.; Haas de Mello, A.; Morris, D.R.; Jones-Hall, Y.L.; Ivanciuc, T.; Sattler, R.A.; Paessler, S.; Menachery, V.D.; Garofalo, R.P.; Casola, A. SARS-CoV-2 Inhibits NRF2-Mediated Antioxidant Responses in Airway Epithelial Cells and in the Lung of a Murine Model of Infection. *Microbiol Spectr* **2023**, *11*, e0037823, doi:10.1128/spectrum.00378-23.

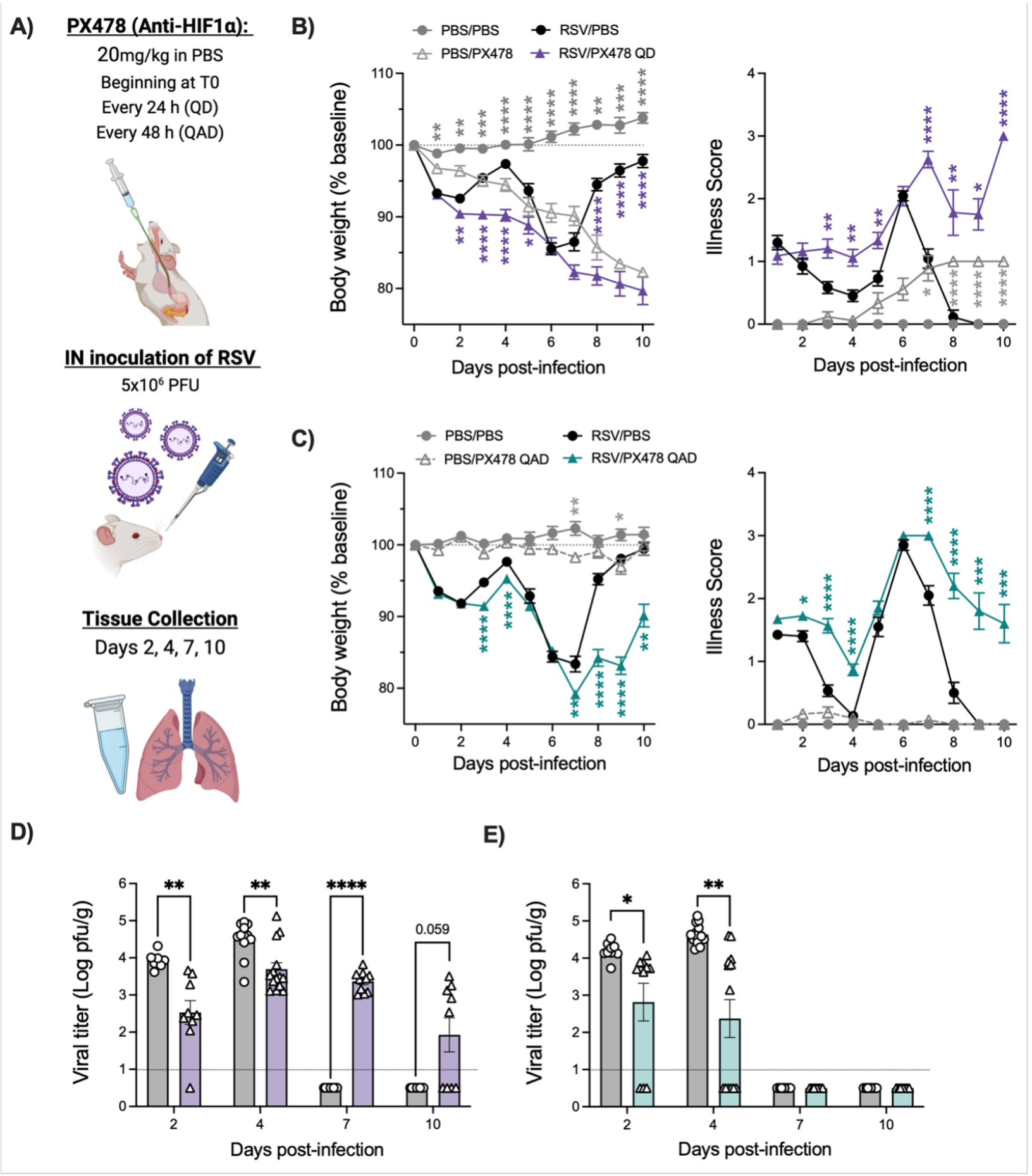
A)
PX478 (Anti-HIF1α):
20mg/kg in PBS
Beginning at T0
Every 24 h (QD)
Every 48 h (QAD)
IN inoculation of RSV
5x10⁶ PFU
Tissue Collection
Days 2, 4, 7, 10
B)
PBS/PBS
RSV/PBS
PBS/PX478
RSV/PX478 QD
Body weight (% baseline)
Days post-infection
Illness Score
C)
PBS/PBS
RSV/PBS
PBS/PX478 QAD
RSV/PX478 QAD
Body weight (% baseline)
Days post-infection
Illness Score
D)
Viral titer (Log pfu/g)
Days post-infection
0.059
E)
Viral titer (Log pfu/g)
Days post-infection

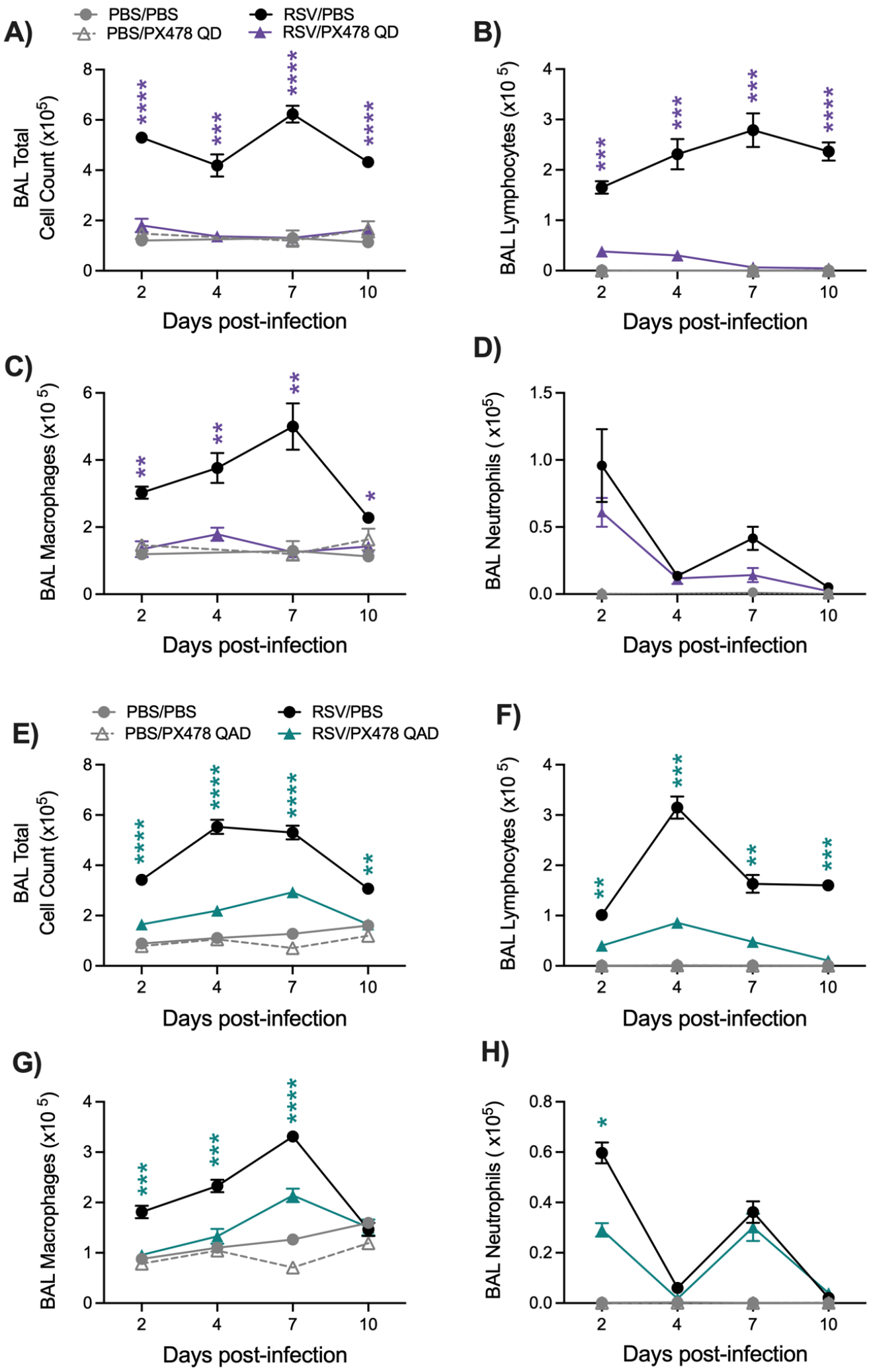
A)
PBS/PBS
PBS/PX478 QD
RSV/PBS
RSV/PX478 QD
BAL Total Cell Count (x10^5)
Days post-infection
B)
BAL Lymphocytes (x10^5)
Days post-infection
C)
BAL Macrophages (x10^5)
Days post-infection
D)
BAL Neutrophils (x10^5)
Days post-infection
E)
PBS/PBS
PBS/PX478 QAD
RSV/PBS
RSV/PX478 QAD
BAL Total Cell Count (x10^5)
Days post-infection
F)
BAL Lymphocytes (x10^5)
Days post-infection
G)
BAL Macrophages (x10^5)
Days post-infection
H)
BAL Neutrophils (x10^5)
Days post-infection

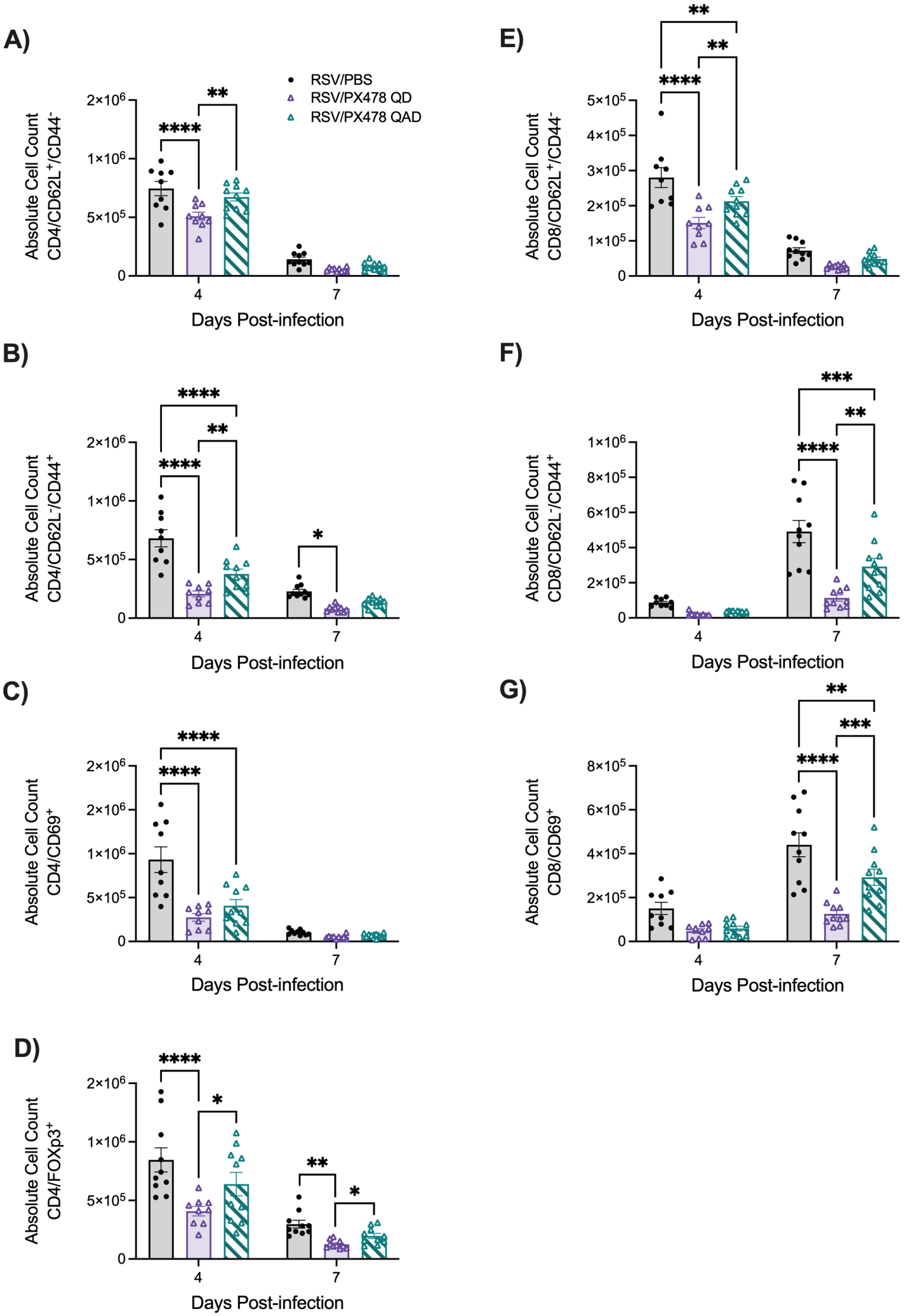
A)
RSV/PBS
RSV/PX478 QD
RSV/PX478 QAD
Absolute Cell Count CD4/CD62L+/CD44-
Days Post-infection
B)
Absolute Cell Count CD4/CD62L-/CD44+
Days Post-infection
C)
Absolute Cell Count CD4/CD69+
Days Post-infection
D)
Absolute Cell Count CD4/FOXp3+
Days Post-infection
E)
Absolute Cell Count CD8/CD62L+/CD44-
Days Post-infection
F)
Absolute Cell Count CD8/CD62L-/CD44+
Days Post-infection
G)
Absolute Cell Count CD8/CD69+
Days Post-infection

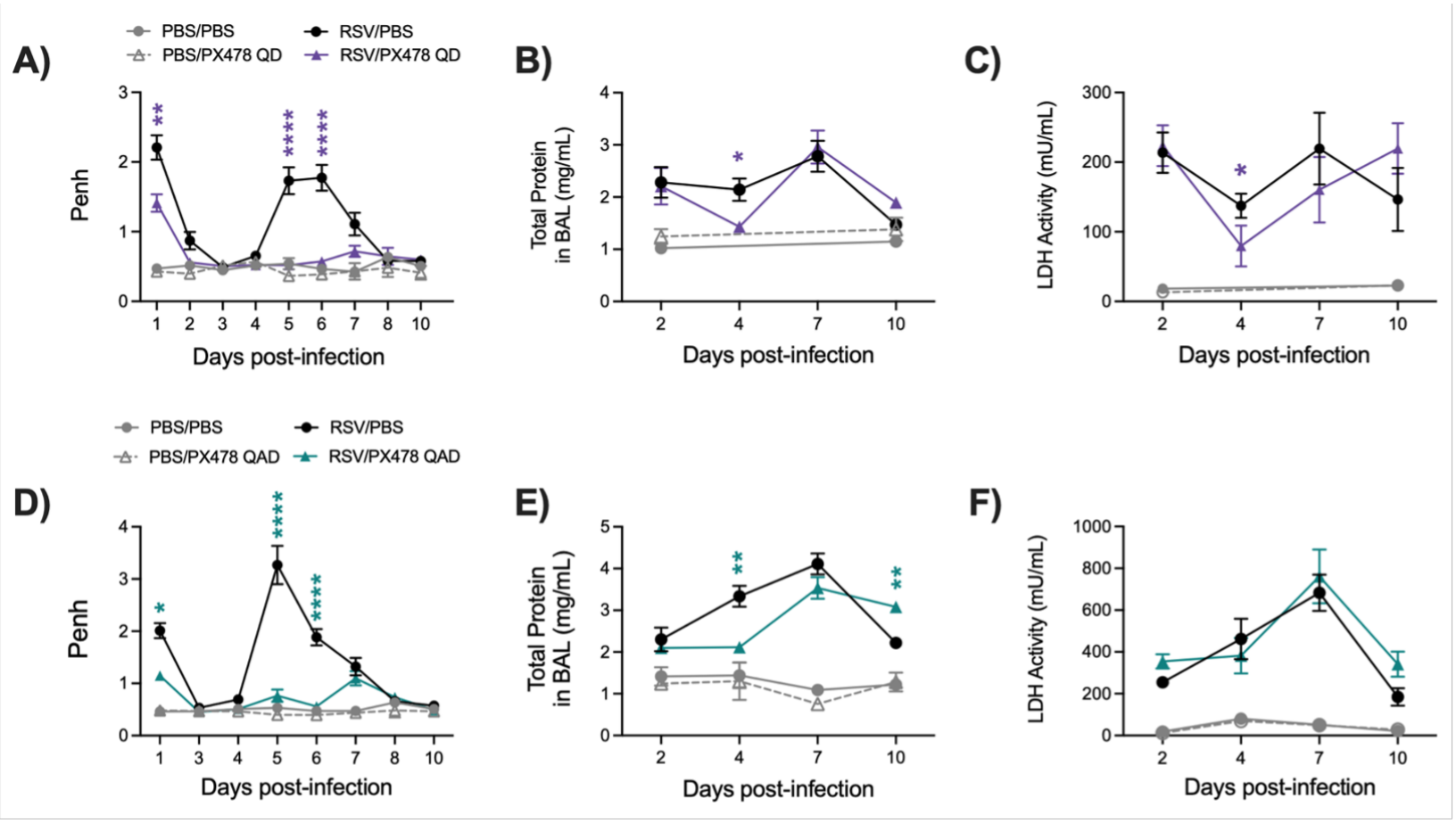
A)
PBS/PBS
RSV/PBS
PBS/PX478 QD
RSV/PX478 QD
Penh
Days post-infection
B)
Total Protein in BAL (mg/mL)
Days post-infection
C)
LDH Activity (mU/mL)
Days post-infection
PBS/PBS
RSV/PBS
PBS/PX478 QAD
RSV/PX478 QAD
D)
Penh
Days post-infection
E)
Total Protein in BAL (mg/mL)
Days post-infection
F)
LDH Activity (mU/mL)
Days post-infection

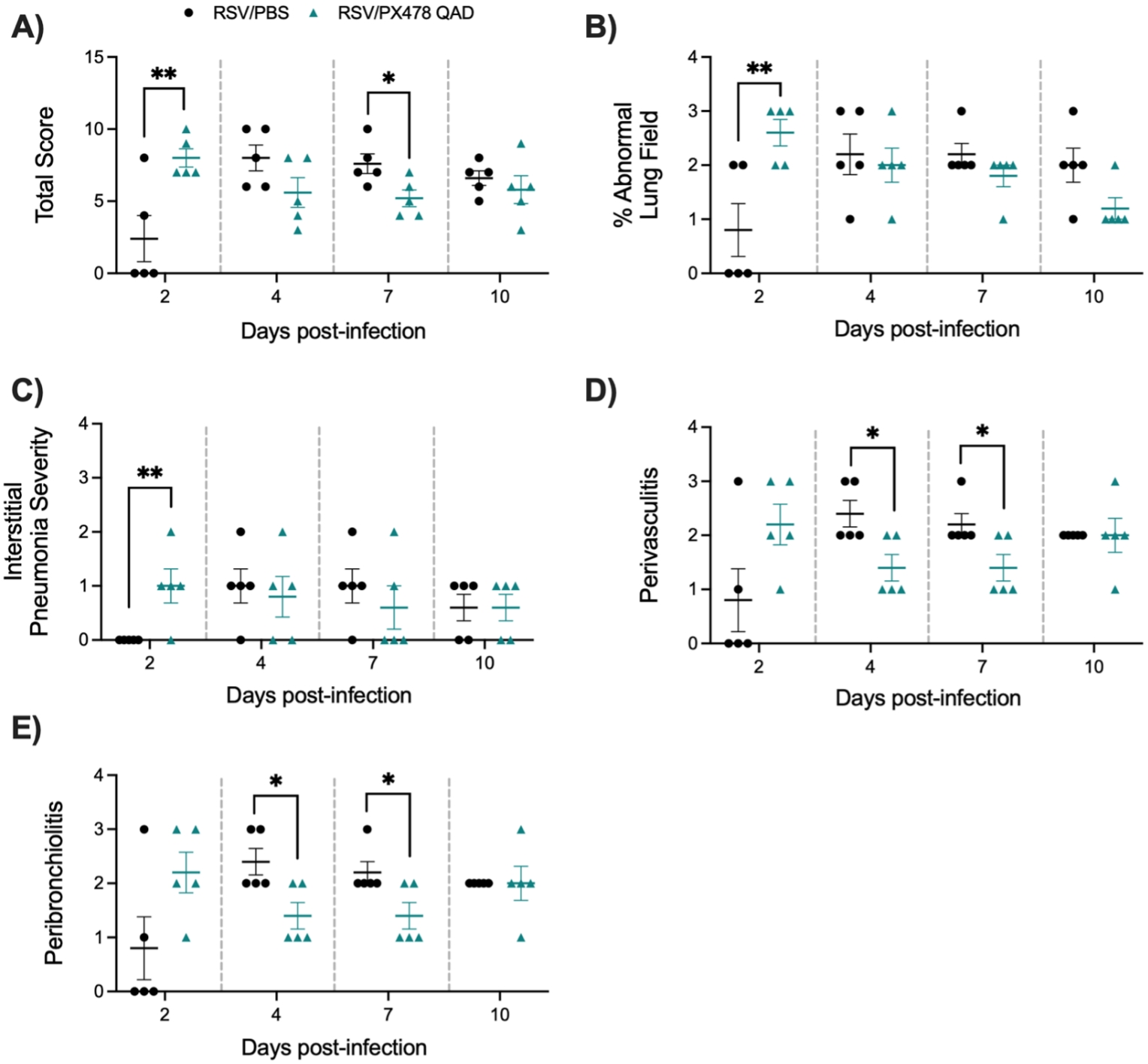
A)
RSV/PBS
RSV/PX478 QAD
Total Score
Days post-infection
B)
% Abnormal Lung Field
Days post-infection
C)
Interstitial Pneumonia Severity
Days post-infection
D)
Perivasculitis
Days post-infection
E)
Peribronchiolitis
Days post-infection

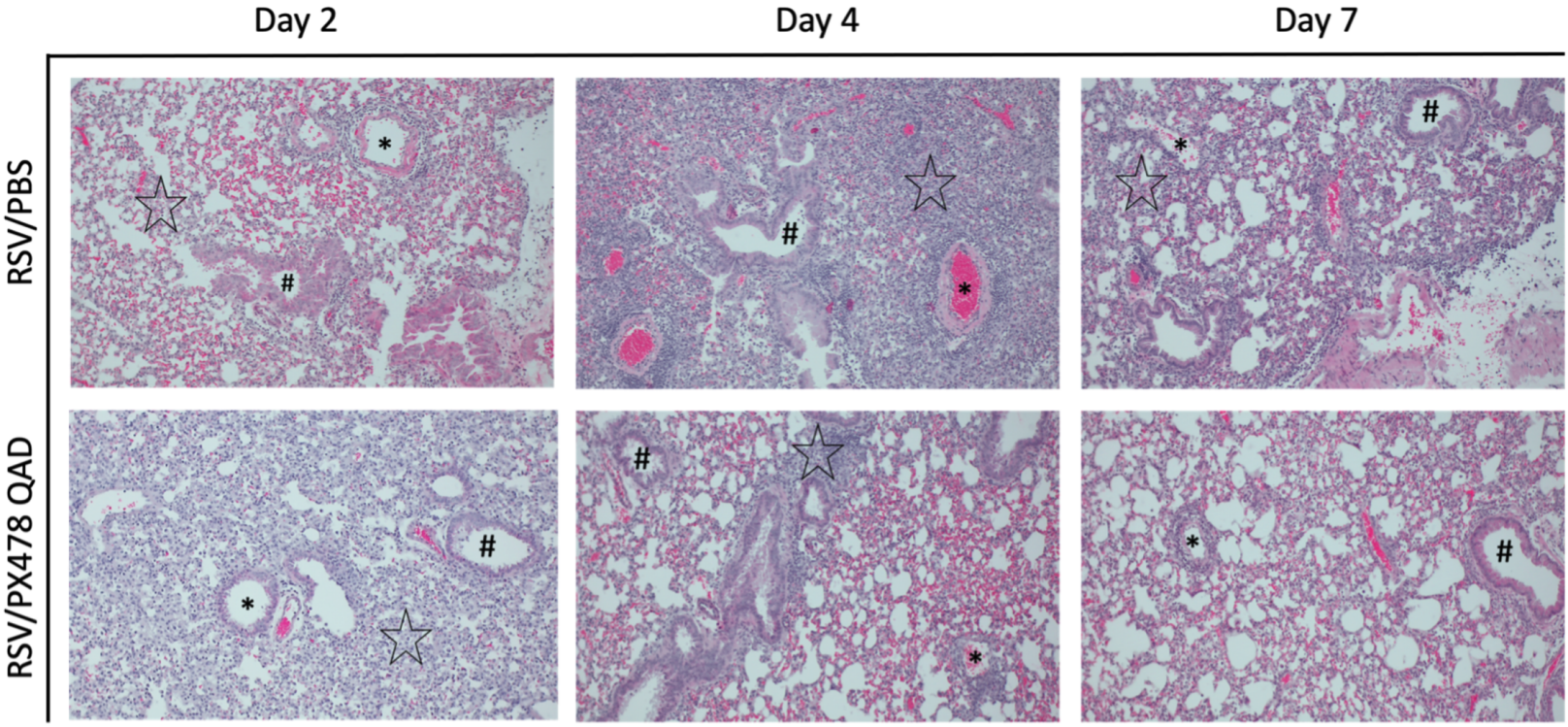
Day 2
Day 4
Day 7
RSV/PBS
RSV/PX478 QAD

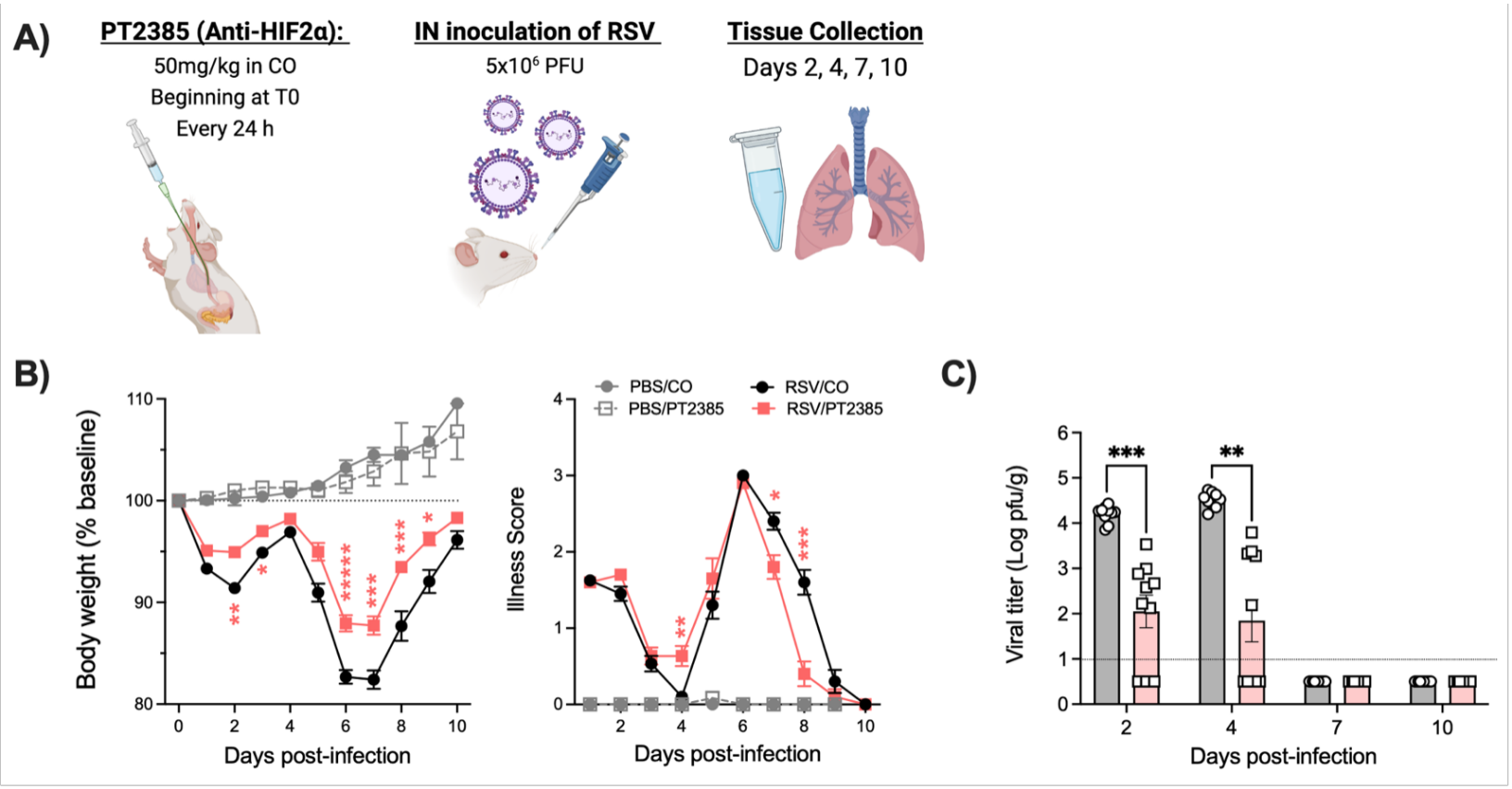
A)
PT2385 (Anti-HIF2α):
50mg/kg in CO
Beginning at T0
Every 24 h
IN inoculation of RSV
5x10⁶ PFU
Tissue Collection
Days 2, 4, 7, 10
B)
Body weight (% baseline)
Days post-infection
Illness Score
Days post-infection
PBS/CO
PBS/PT2385
RSV/CO
RSV/PT2385
C)
Viral titer (Log pfu/g)
Days post-infection

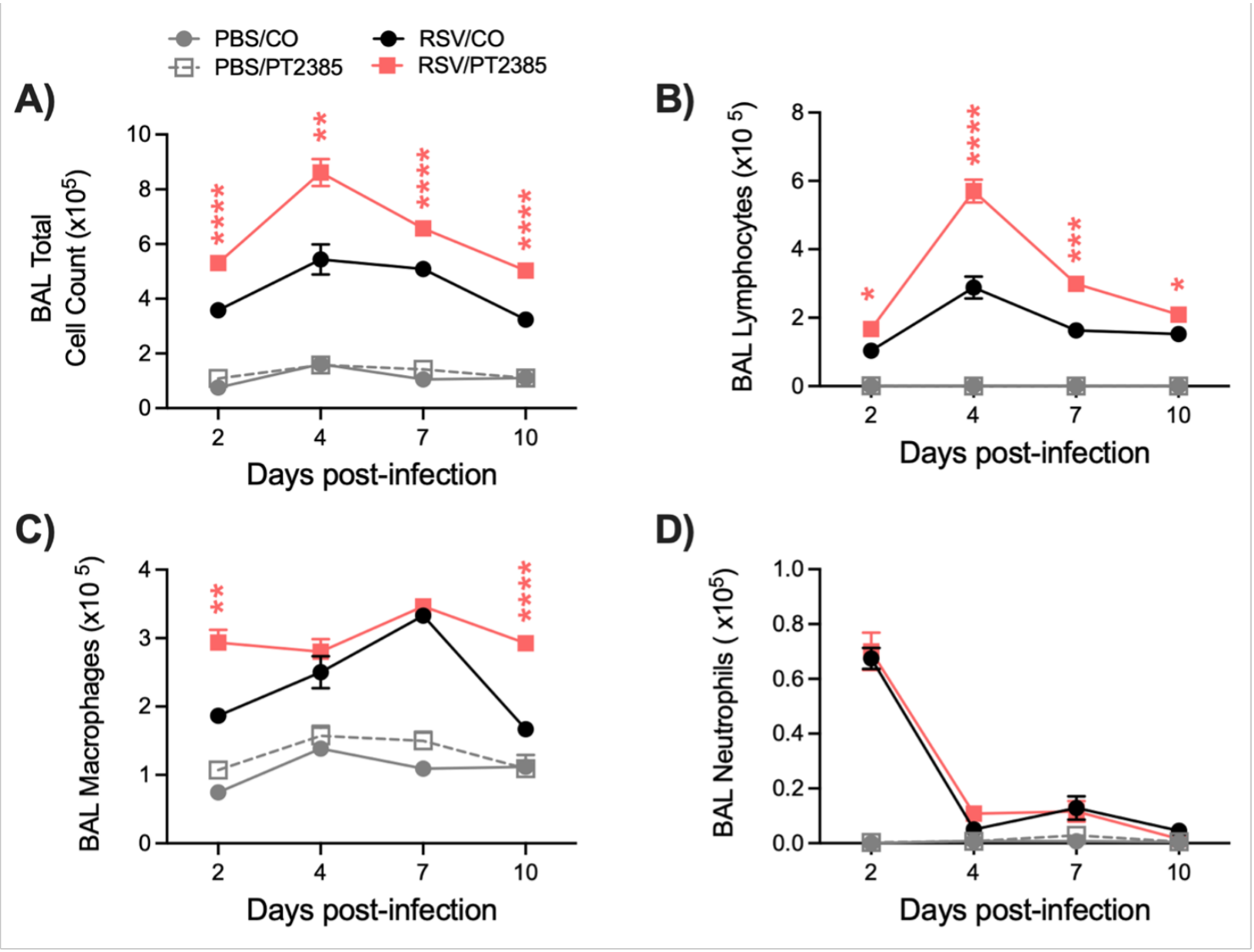
PBS/CO
PBS/PT2385
RSV/CO
RSV/PT2385
A)
BAL Total Cell Count (x10^5)
Days post-infection
B)
BAL Lymphocytes (x10^5)
Days post-infection
C)
BAL Macrophages (x10^5)
Days post-infection
D)
BAL Neutrophils (x10^5)
Days post-infection

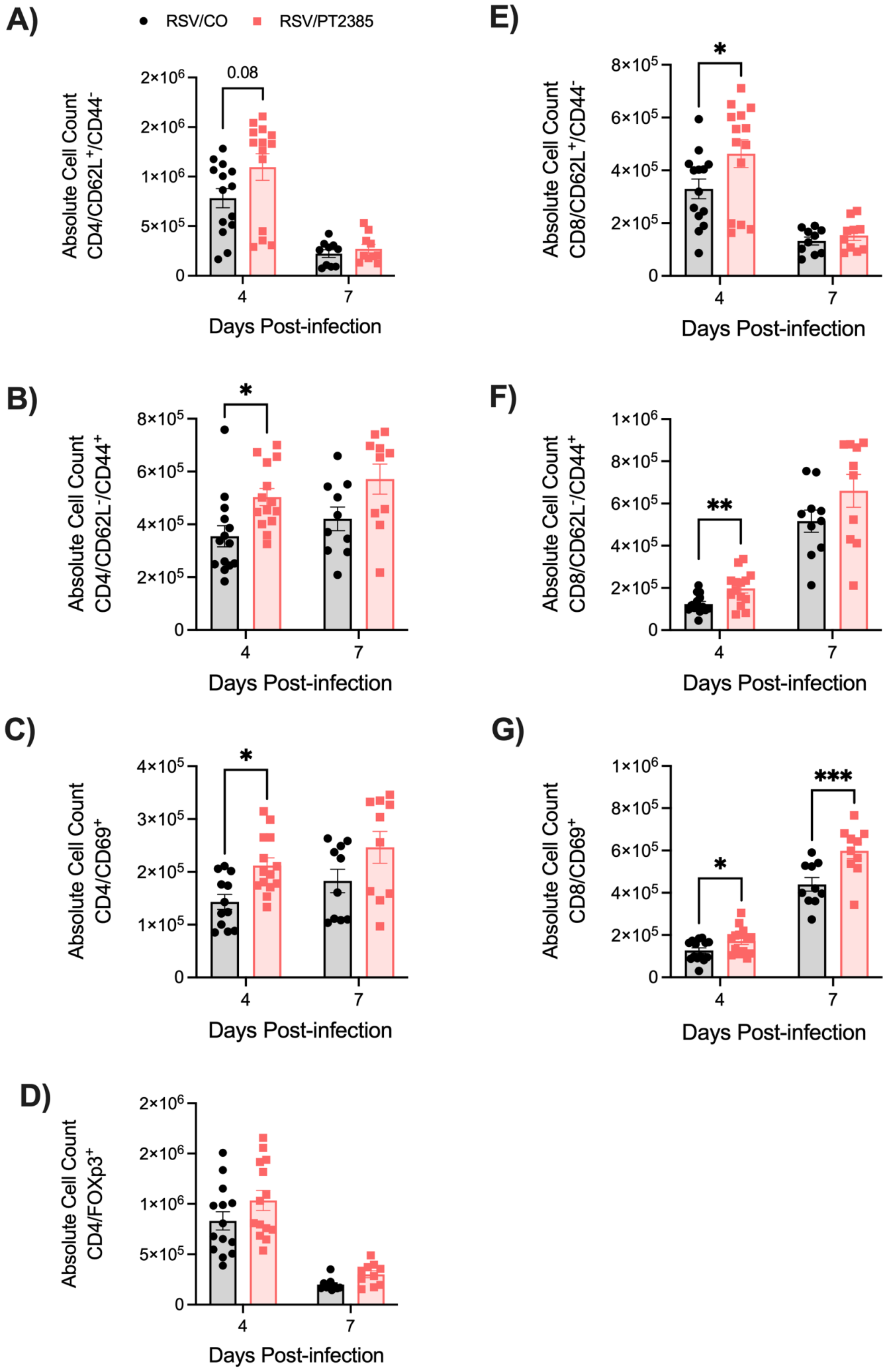
A)
RSV/CO
RSV/PT2385
0.08
Absolute Cell Count CD4/CD62L+/CD44-
Days Post-infection
B)
*
Absolute Cell Count CD4/CD62L-/CD44+
Days Post-infection
C)
*
Absolute Cell Count CD4/CD69+
Days Post-infection
D)
Absolute Cell Count CD4/FOXp3+
Days Post-infection
E)
*
Absolute Cell Count CD8/CD62L+/CD44-
Days Post-infection
F)
**
Absolute Cell Count CD8/CD62L-/CD44+
Days Post-infection
G)
*
***
Absolute Cell Count CD8/CD69+
Days Post-infection

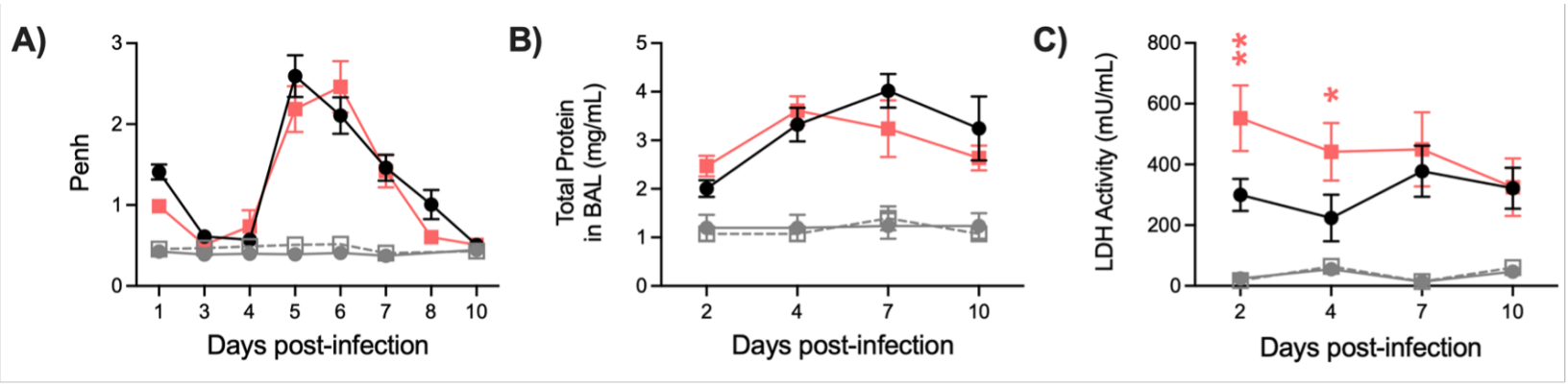
A)
Penh
Days post-infection
B)
Total Protein in BAL (mg/mL)
Days post-infection
C)
LDH Activity (mU/mL)
Days post-infection

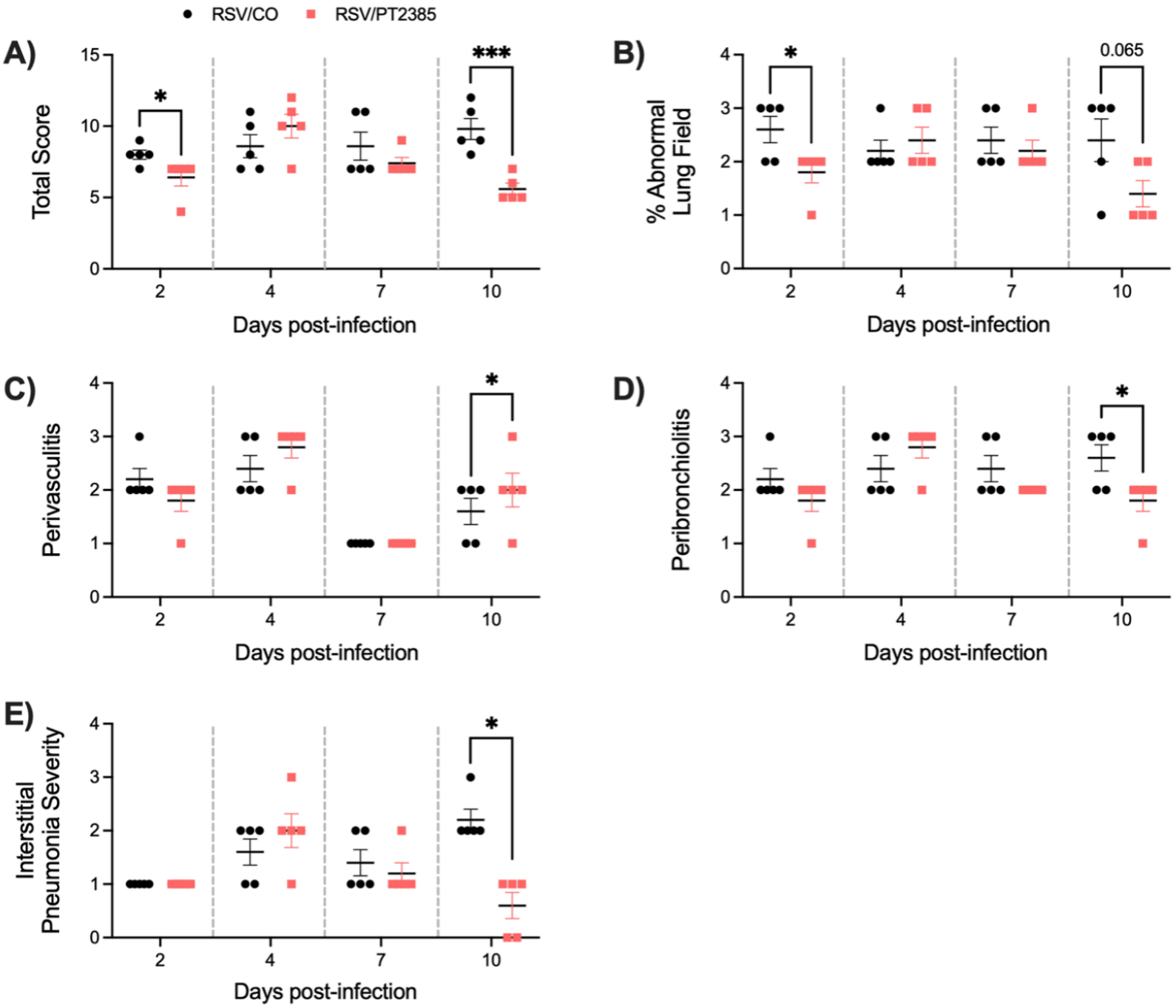
RSV/CO
RSV/PT2385
A)
Total Score
*
***
Days post-infection
B)
% Abnormal Lung Field
*
0.065
Days post-infection
C)
Perivasculitis
*
Days post-infection
D)
Peribronchiolitis
*
Days post-infection
E)
Interstitial Pneumonia Severity
*
Days post-infection

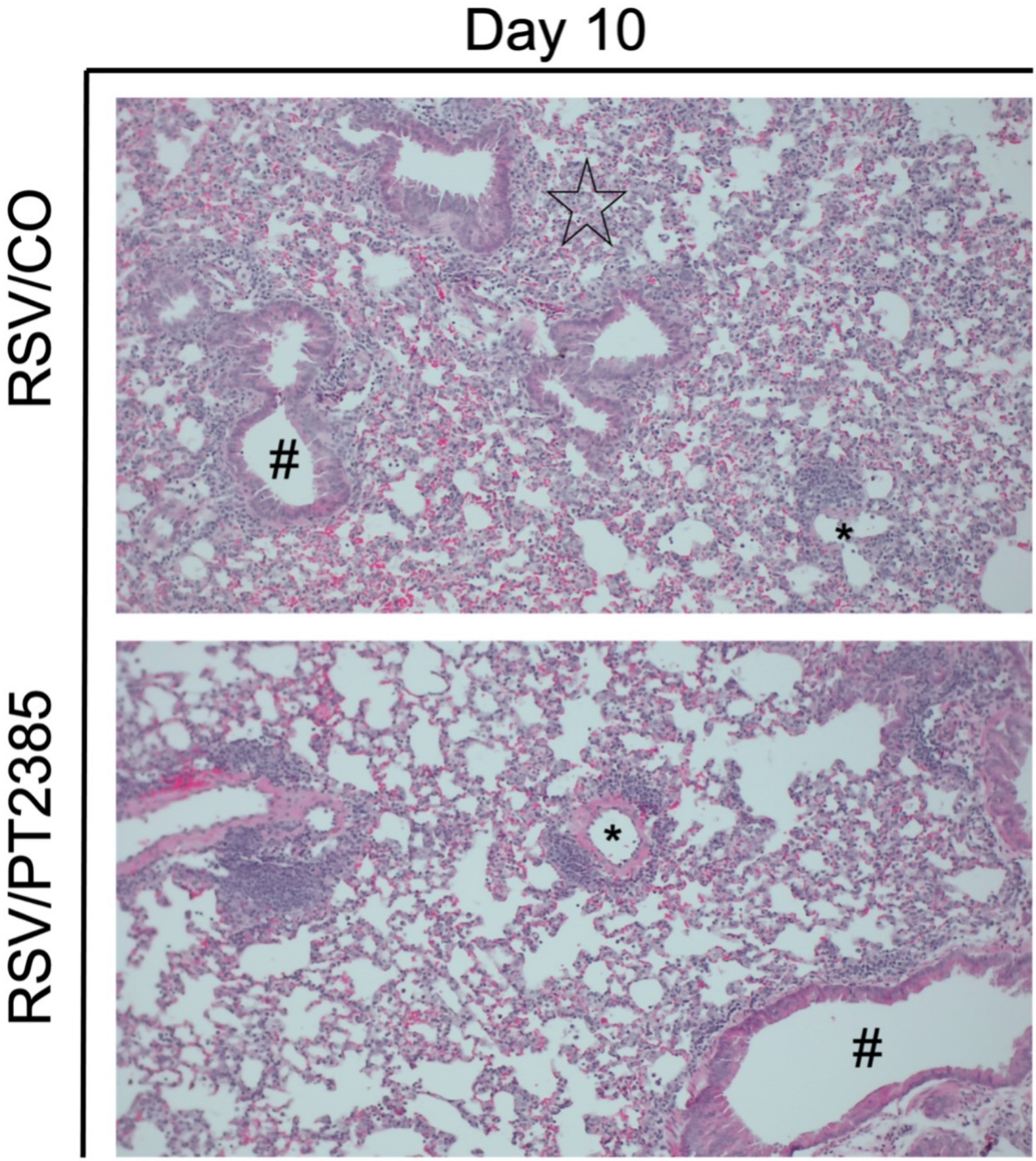
Day 10
RSV/CO
RSV/PT2385
#
*
*
#